C. R. Physique 16 (2015) 118–138

Contents lists available at ScienceDirect

Comptes Rendus Physique

www.sciencedirect.com

Granular physics / Physique des milieux granulaires

Dune morphodynamics

Morphodynamique des dunes

Sylvain Courrech du Pont

Laboratoire "Matière et systèmes complexes", Sorbonne Paris Cité, Université Paris-Diderot, CNRS UMR 7057, 10, rue Alice-Domon-et-Léonie-Duquet, 75205 Paris cedex 13, France

ARTICLE INFO

Article history:
Available online 18 February 2015

Keywords:
Dune
Geomorphology
Desert
Barchan
Sand transport
Collective motion

Mots-clés :
Dune
Géomorphologie
Désert
Barchane
Transport de sable
Mouvements collectifs

ABSTRACT

The physics of dunes relies on the interaction between a wind flow and an erodible topography. Thus, if strong enough to transport grains, the wind shapes sandy areas into dune fields. These dunes are reminiscent of a wavy sea so that sandy deserts are called sand seas. However, the comparison stops there. Contrary to water waves, dunes propagate only under wind action and when the wind stops, they do not vanish but stand. Consequently, dunes are not only the result of the present winds, but can integrate the wind regimes over long periods. Thus, they exhibit a range of shapes and sizes with superimposed patterns. They are witnesses of past wind regimes and their shape and orientation are used to constraint climatic models on other planetary bodies where they are observed as well (e.g., Mars, Titan and Venus). Here, we discuss the morphodynamics of dunes and endeavor to identify and to explain the physical mechanisms at play in the selection of their shape, size and orientation, whilst focusing on Earth desert sand dunes.

RÉSUMÉ

La physique des dunes repose sur l'interaction entre le vent et une topographie érodable. Quand le vent souffle au-dessus d'une surface de sable, des dunes se forment dès lors que des grains sont transportés. Ces dunes offrent un paysage qui ressemble à une mer mouvementée et les déserts sableux sont appelés des mers de sable. Cependant, l'analogie entre dunes et vagues s'arrête là. Contrairement aux vagues, les dunes ne se propagent que sous l'action du vent, et si le vent s'arrête de souffler, elle ne disparaissent pas, mais persistent. Ces tas de sable ne sont pas seulement le fruit des vents présents, mais peuvent intégrer l'histoire des vents sur de longues périodes. Cette propriété explique la richesse des formes et des échelles observées, et fait des dunes des témoins des vents passés. Ainsi, on utilise leur forme et surtout leur orientation pour contraindre les modèles climatiques des corps célestes comme Titan, Mars ou Vénus, où elles sont observées. Dans cet article, nous expliquons la forme, la taille et l'orientation des dunes en passant en revue la littérature récente et en nous attachant à identifier et à expliquer les mécanismes physiques mis en jeu.

E-mail address: sylvain.courrech@univ-paris-diderot.fr.

http://dx.doi.org/10.1016/j.crhy.2015.02.002
1631-0705/

The physical study of dunes started with the seminal work of Ralph A. Bagnold [1], who found interest in the shape of dunes and in Aeolian sand transport, while stationed in Egypt and Libya as an officer of the British Army between World War I and World War II [2]. Since then, great progress has been achieved by the increasingly joint effort of a vast scientific community among Earth Sciences and Physics. Moreover, the abundance and free access to satellite images and meteorological data have allowed field remote studies, which is valuable to easily test models. The lushness of the physics of dunes stands in the permanent feed-back between the dunes topography, the air flow and the sediment transport. Carrying on the subject from start and at the light of recent studies, we aim to give a comprehensive and consistent picture of dune morphodynamics in Earth sandy deserts. In the first section, we present the main properties of turbulent wind flow and sand transport. In the second section we explain the genesis of dunes growing from the destabilization of a sand bed. In the third section, wind regimes in sandy deserts are quickly overviewed. In the fourth and main section we explain the shape, the orientation and the size of dunes. In the fifth section, we finally discuss the dynamics of a dune field.

1. Sand transport over a flat sand bed

1.1. Turbulent flow over a flat ground

For a steady unidirectional turbulent flow (high Reynolds numbers) over a flat bottom extending in the x direction at $z = 0$, the average fluid velocity component along x, u, increases with the logarithm of the distance z to the bottom [3]:

$$u(z) = \frac{u_*}{\kappa} \ln\left(\frac{z}{z_0}\right) \tag{1}$$

where $\kappa \simeq 0.4$ is the von Kármán constant, u_* the friction velocity and z_0 the roughness length. This equation, which is verified experimentally for a non-stratified fluid [4], arises from the different nature of the transport of momentum and from the lack of a characteristic length scale in turbulence. According to the Prandtl theory, the transport of momentum is not driven by the thermal agitation on a characteristic length set by the mean free path of gas molecules, but by the fluid velocity fluctuations on a mixing length of the order of the distance to the bottom. As in a laminar viscous simple shear flow, the shear stress or momentum flux τ_{xz} is constant and imposed by the bottom. Here τ_{xz} is equal to the friction stress: $\tau_{xz} = \rho_f u_*^2$, where ρ_f is the volume mass of the fluid, and the friction velocity u_* relates to the root-mean-square of the velocity fluctuations along z [3]. Eq. (1) does hold very close to the ground. Just above the ground, where the velocity is zero, lies a viscous boundary layer where the velocity profile along the z-axis is linear. The viscous boundary layer extends to a height l_v where the two modes of momentum transport match, i.e. where $\rho_f u_*^2 \sim \eta u_*/l_v$. When the fluid is air ($\rho_f \simeq 1.2\ \mathrm{kg\,m^{-3}}$, viscosity: $\eta \simeq 1.8 \cdot 10^{-5}$ Pa s), taking u_* equal to a typical value of transport threshold velocity of $0.2\ \mathrm{m\,s^{-1}}$ gives $l_v \sim 75$ µm. Although l_v is not negligible compared to the diameter d of sand grains ($d \simeq 100$–300 µm), the transport does not take place in the viscous layer in the air. Nevertheless, when the surface is smooth, l_v sets the value of the aerodynamic roughness z_0. However, dunes are not smooth and z_0 is rather set by (equals a fraction of) the size of sand grains, the length of ripples or by the thickness of the transport layer [1].

1.2. Onset of transport

The fluid velocity has to overcome a critical value in order to set grains into motion. Before the transport onset, the forces acting on a sand grain trapped between its neighbors are the weight, the buoyancy, the Coulomb static friction, the bed reaction, possible cohesive forces (van der Waals or capillary forces) and the fluid drag and lift forces. A grain is set into motion when the equilibrium of forces (or torques) is broken. Assuming no cohesion and considering the granular sand bed as a continuous medium, the onset of transport can write as a balance between the bottom fluid shear stress τ and a solid Coulomb friction force per unit of area. This latter is proportional to the apparent weight of a grain-diameter-thick sand layer per unit of area, multiplied by a macroscopic friction coefficient μ. μ relates to the granular packing geometry (traps) and the granular angle of movement rather than to the grain–grain friction coefficient. Assuming that neither μ nor the packing fraction of the granular layer depends on the fluid, the grains' properties or the flow regime, the transport onset corresponds to a critical value of a dimensionless ratio Sh called the Shields number:

$$Sh = \frac{\tau}{(\rho_s - \rho_f) g\, d} \tag{2}$$

where ρ_s is the sand volumic mass and g the gravity acceleration. For a turbulent flow in the air, a constant Shields number with $\tau = \rho_f u_*^2$ fairly describes the experimental measurements of transport onsets [5] provided that grains are large enough not to lie in the viscous sublayer of the flow ($d \gg l_v$). When the wind speed further increases, the number of grains into motion increases. The transported grains impact the static bed and share a part of their momentum, which helps to untrap static grains. Thus, there is a dynamic threshold fluid velocity u_d, which is smaller than the static one and is relevant to describe the sand flux. If impacts play a bigger role than the fluid flow, one can argue that the threshold impacting grain velocity, which is proportional to the fluid velocity u_d, is the typical velocity to dislodge a grain from its trap. Then, u_d scales with the grain size, so that $u_d \propto \sqrt{gd}$ [6–8] and the corresponding dynamic onset Shields number Sh_d depends on

fluid and grain densities. However, one can rather imagine that an impact should be energetic enough to elevate a grain not on a trap height, but on a sufficient height so that the ejected (or rebounding) grain gets time for being reaccelerated by the fluid flow. Thus, the characteristic height and length of a grain trajectory at transport threshold are proportional to the inertia length: $l_{\mathrm{drag}} = \rho_{\mathrm{s}} d/\rho_{\mathrm{f}}$, which leads to:

$$u_{\mathrm{d}} \propto \sqrt{(\rho_{\mathrm{s}} - \rho_{\mathrm{f}}) g\, d/\rho_{\mathrm{f}}} \tag{3}$$

It corresponds to a constant dynamic onset Shields number Sh_{d} independent of fluid and grain densities. For desert sand grains in the air ($d \simeq 200$ µm), u_{d} is about 20 $\mathrm{cm\,s^{-1}}$, which corresponds to a wind speed of about 4.5 $\mathrm{m\,s^{-1}}$ ten meters above the ground. Note that the dynamic threshold is less relevant for transport in water, where the restitution coefficient of impacting grains is much smaller [9].

1.3. Motion of transported grains

Grain motions can be categorized into 3 groups: saltation (grains that make successive jumps and have a ballistic trajectory), creeping motion or bed load (rolling grains or ejected grains when grains in saltation impact the sand bed) and suspension (grains that are elevated much higher above the bed and travel long distances). Only creeping motion and saltation are relevant for dune dynamics. This sand transport occurs in a surface layer, which is a few centimeters thick [10,11].

1.4. Saturated sand flux

Although the wind over a sand bed is turbulent and intermittent, the sand flow is believed to reach a constant value called the saturated sand flux. In the air, the transport in saltation occurs in a thin layer above the ground. Above this transport layer, the logarithmic profile of the fluid velocity (Eq. (1)) still holds but with a roughness length z_0 that increases with the fluid velocity u_* and the corresponding increasing sand transport [1,12]: the sand transport slows down the wind. The saturated sand flux corresponds to an equilibrium, which can write as a momentum flux balance [13,14,6,7]. Grains in saltation lose a part of their momentum when impacting the sand bed. Thus, to keep the transport at the saturation value, the fluid has to re-accelerate grains along their saltation path from their lifting velocity to an impacting velocity, which is just large enough to create a new sustainable saltation motion, i.e. the threshold impacting grain velocity. Therefore, both lifting and impacting velocities differ by a restitution coefficient factor and are proportional to the dynamic threshold velocity u_{d}, which is consequently also the velocity at which the fluid has been reduced in the transport layer:

$$\rho_{\mathrm{f}} u_*^2 - \rho_{\mathrm{f}} u_{\mathrm{d}}^2 = \rho_{\mathrm{s}} q_{\mathrm{sat}} \frac{\Delta v}{l_{\mathrm{h}}} \tag{4}$$

The left-hand side is the momentum flux the fluid gives to sustain the transport in the transport layer. q_{sat} is the saturated sand flux integrated on the transport layer height. It has the dimension of a surface per unit of time and takes into account the packing fraction of the granular arrangement of the sand bed. Δv is the difference between averaged impacting and lifting grain velocities, formally perpendicular to the flow direction. l_{h} is the mean saltation length (from lift to impact) on which the fluid drag force works to re-accelerate a grain, and the characteristic length to "renew" the population of grains in saltation. In the above-developed picture, $\Delta v \propto u_{\mathrm{d}}$ and so does the grains lifting vertical velocity. Grains are returned to the ground by the gravity, so that the saltation length l_{h}, like the transport layer thickness, scales like: $l_{\mathrm{h}} \propto u_{\mathrm{d}}^2\, \rho_{\mathrm{s}}/[(\rho_{\mathrm{s}} - \rho_{\mathrm{f}})g]$. This leads to:

$$q_{\mathrm{sat}} \propto u_{\mathrm{d}}\, \frac{\rho_{\mathrm{f}}}{(\rho_{\mathrm{s}} - \rho_{\mathrm{f}})g} \left(u_*^2 - u_{\mathrm{d}}^2\right) = d\, u_{\mathrm{d}}\, (Sh - Sh_{\mathrm{d}}) \tag{5}$$

which was first proposed by Ungar and Haff [8] with $u_{\mathrm{d}} \propto \sqrt{g\, d\, (\rho_{\mathrm{s}} - \rho_{\mathrm{f}})\,/\,\rho_{\mathrm{s}}}$, but here we set $u_{\mathrm{d}} \propto \sqrt{(\rho_{\mathrm{s}} - \rho_{\mathrm{f}}) g\, d/\rho_{\mathrm{f}}}$ (Eq. (3)). Eq. (5) assumes that transported grains are in saltation within a layer in which the fluid flow has been reduced to the transport onset conditions. The number (or mass) of transported grains increases with the square of the fluid velocity, like $(Sh - Sh_{\mathrm{d}})$, but their mean velocity remains constant and set by u_{d}. In Earth deserts, the wind velocity is rarely stronger than 2 or 3 times the threshold velocity. In such conditions, experiments [10,11] and numerical simulations [6] have shown that the thickness of the transport layer ($\sim$ 1–2 cm) [10,11] as the velocity of transported particles [12,15,6] are roughly independent on the fluid velocity u_*. Thus, when the fluid velocity increases, only the density of particles in motion inside the transport layer increases [10,16]. For fast flows ($u_* > 4\, u_{\mathrm{d}}$, [6]) or on non-erodible grounds [15], this picture does not hold and the saturated sand flux rather scales with u_*^3, which is the dependence of many other models, all partly empirical or phenomenological [1,14,17]. Such a scaling corresponds to the picture of a dilute transport layer, which expands when the fluid velocity increases and barely slows the fluid flow down [6].

1.5. Saturation length

If the wind accelerates (or decelerates), the sand flux does not adapt instantaneously. The flow needs a given distance, the saturation length l_{sat}, to load in grains so that the sand flux reaches the saturated value (Fig. 1). One may think at

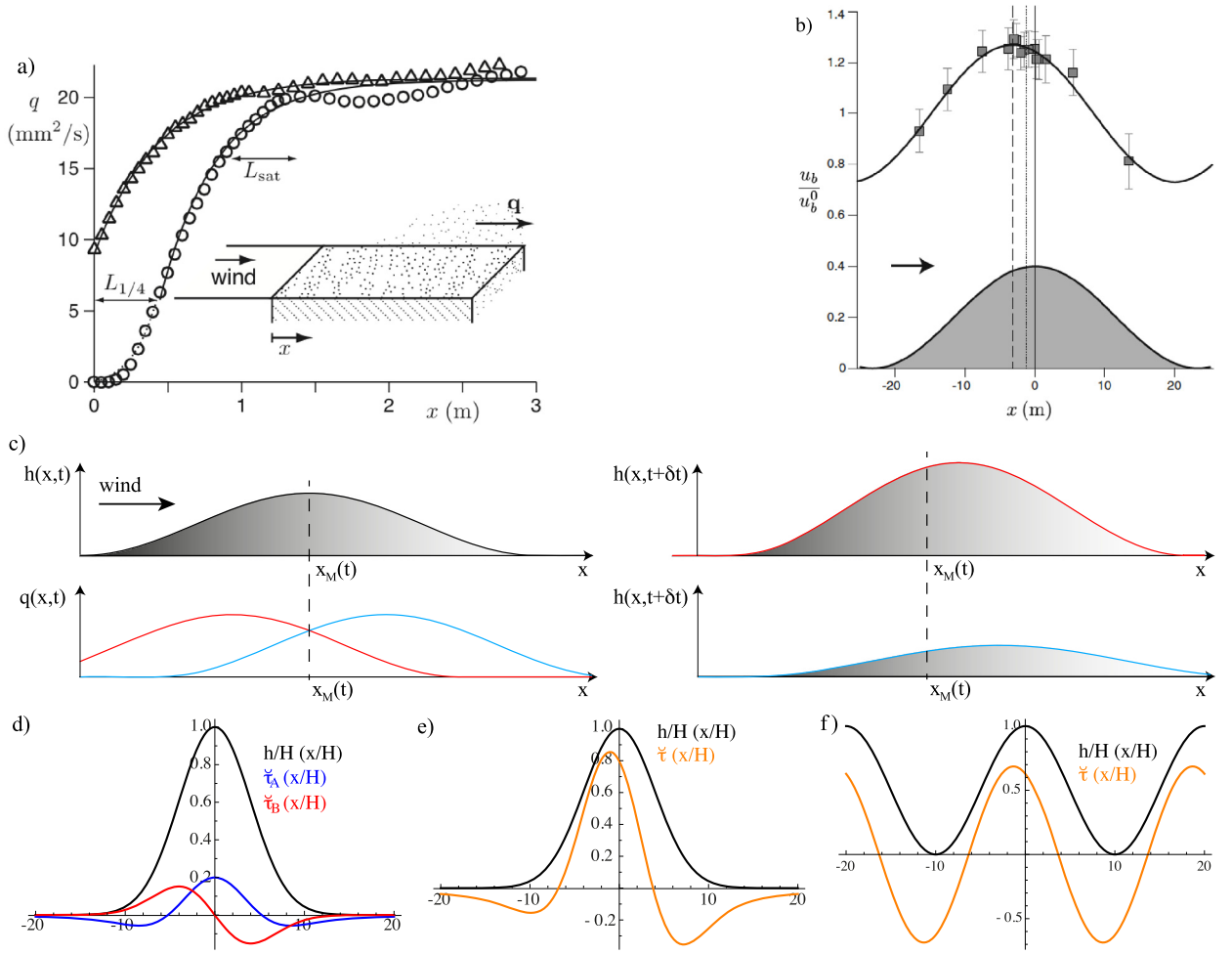

Fig. 1. (Color online.) a) Spatial variation of the sediment flux over a flat sand bed in a wind tunnel. The sand bed starts at $x = 0$, triangles (resp. circles) correspond to an experiment with (resp. without) an input flux [21]. b) Longitudinal profile of the wind speed u_b, measured 11 cm above the surface of a low dune. u_b is normalized by u_b^0, the fitted value of u_b at mid-height. The arrow shows the wind direction. The dune profile is reasonably fitted by a cosine shown in grey at the bottom of the graph. The velocity is maximum upwind from the top of the dune [22]. c) Sketch of the instability of a dune, sand flux $q(x)$ over a dune topography $h(x)$. The dune increases in height if the sand flux is maximum before the summit x_M (red) and decreases if the sand flux is maximum after the summit (blue). d) "A" (in phase) and "B" (out of phase) terms of the bottom shear stress perturbation $\breve{\tau}$ (Eq. (7)) over a Gaussian profile $h(x)/H = \exp[-x^2/(2c^2)]$ with $c = 4H$. e) Bottom shear stress perturbation $\breve{\tau}$ (Eq. (7)) over a Gaussian profile $h(x)/H = \exp[-x^2/(2c^2)]$ with $c = 4H$, $A = 4$ and $B = 1.75$. f) Bottom shear stress perturbation $\breve{\tau}$ (Eq. (7)) over a cosine profile $h(x)/H = (1/2)[1 + \cos(2\pi x/\lambda)]$ with $\lambda = 20H$, $A = 4$ and $B = 1.75$. The bottom shear stress is maximum before the top of the bump. The maximum value of the shear stress perturbation is substantial for bumps of aspect ratio $H/(2c) = 1/8$ or $2H/\lambda = 1/10$ (alike dunes). Note the difference of the minimum $\breve{\tau}$ obtained for a wavy topography in f) and an isolated bump in e).

several characteristic distances for l_{sat}: the saltation length l_h, the characteristic length l_{drag} for a grain to be accelerated to the fluid velocity or an inertia length for the fluid flow, which has to decelerate to the transport onset velocity. Since we are considering a relaxation process (the sand flux is close to its saturated value), the longest of these lengths controls the saturation length. As we saw, all the above lengths are comparable and scale like the drag length l_{drag} [18,19]. Although one cannot completely exclude a dependence in wind speed [20], measurements in typical wind conditions on Earth ($u_* \simeq 1 - 3u_d$) are in good agreements with $l_{sat} \simeq 2\,d\,\rho_s/\rho_f$, which ranges from 40 to 120 cm in the air for sand grains of diameter ranging from 100 to 300 μm [21].

2. Genesis and minimum size of dunes—instability of a sand bed

Dunes are ubiquitous on Earth and experiments have shown that a flat sand bed, sheared by a fluid flow, destabilizes into propagating dunes as soon as the flow transports grains [23–27]. The incipient dunes develop with a well-defined wavelength. These observations are signatures of a supercritical and convective instability (whatever the height of the perturbation, a bump will grow) with a dominant unstable wavelength (the one of incipient dunes). Furthermore, no dunes smaller than a critical length (∼ 6–10 m) are observed on Earth [1], which indicates that small wavelengths are stable.

Let us consider a pile on a sand bed as shown in Fig. 1c. Above the pile, the fluid flow speeds up, which modifies the sand transport. The bump increases in height if sand is deposited at the top, i.e. if the top is a place where the sand flux is decreasing. Thereby, the instability develops and a dune grows if the maximum sand flux is reached before the bump top. Conversely, the bump flattens and vanishes if the sand flux is spatially in delay with the topography. The time scale over which the dune topography changes is much longer than the time for the fluid flow or the sand transport to adapt to a topography. Hence fluid flow and sediment transport can be considered stationary (on a time scale longer than the characteristic time of turbulent fluctuations).

2.1. Fluid flow over a flat bump or a smooth wavy floor

As transport occurs in a thin layer above the sand bed, we focus on the fluid velocity a few centimeters above the ground. The velocity over a model-hill has been measured in a wind tunnel by Gong and Ibbetson [4] and recently above a flat dune in the field by Claudin et al. [22]. These measurements in the turbulent regime show an upwind shift of the maximum flow velocity with respect to the topography when measuring close to the surface (Fig. 1). Higher above the ground, the velocity is slightly in lag with the topography profile [28,29]. There, well above the surface, the flow is dominated by inertia and speeds up above a bump because of mass conservation—the confinement is due to the upper flow itself. Closer to the bed, the turbulent bottom shear stress controls the flow. The thickness of this inner layer l_t corresponds to the height where longitudinal inertia ($\sim u^2/L$) balances the divergence of the turbulent stress ($\sim u_*^2/l_t$), so that:

$$\frac{l_t}{L}\ln^2(l_t/z_0) \sim \kappa^2 \tag{6}$$

where L is the bump length [30]. Taking the typical values $L = 30$ m and $z_0 = 1$ mm gives $l_t \sim 15$ cm, which is relevant for the transport of grains in saltation. The upwind phase shift of the fluid velocity holds close to the ground in the turbulent inner layer and is a local effect. A positive bed slope imposes more resistance to the flow than a negative slope. The friction stress increases with the bed slope and so does the fluid velocity in the inner layer as the two are intrinsically linked. Analogously, one can have the picture of the fast fluid from the upper layers accelerating by advection the flow in the inner layer. This effect is all the more important that the inner layer, which follows the topography, is positively tilted compared to the main flow direction. At the bump summit the slope is zero, so that the fluid velocity in the inner layer is maximum before the summit. This phase advance, which explains the bed instability, is not specific to turbulent flows and dunes are observed in laminar flow regimes [32].

More formally, in the outer region well above the ground, the flow can be considered as an inviscid potential flow. Inertia and pressure gradient balance. As a result for a smooth topography with a small aspect ratio, the flow is in phase with the topography. The velocity is maximum above the summits and minimum above the troughs. It is the opposite for the pressure (Bernoulli's principle), which is minimum above the summits and maximum above the troughs. Along a streamline, the absolute value of the driving pressure gradient is maximum where the velocity accelerates the most and then is phase shifted in regard to the topography. In the turbulent inner layer, the flow velocity is reduced because of the friction with the bottom and the fluid inertia is no more relevant. There, the fluid flow is accelerated by the transverse turbulent transport of momentum from the outer region to the inner layer (in phase) and by the longitudinal pressure gradient inherited from the outer flow, which holds in the inner layer (phase shifted).[1] On a theoretical point of view, the bumpy bed is considered as a small perturbation to a flat bed, which involves a small perturbation to the fluid velocity. The flow can be divided into distinct regions (in height) where the flow response to the bed perturbation are driven by different mechanisms and that have to be combined. Jackson and Hunt [33] did such a calculation (asymptotic matching), which has been simplified by Kroy et al. to model dunes [34] and strengthened in several ways by Fourrière et al. [35]. The perturbation $\check{\tau}(x)$ of the bottom shear stress $\tau(x)$ or equivalently of the square of the characteristic friction velocity $u_*(x)$ in the inner layer, perturbed by a bed profile $h(x)$, then reads:

$$\check{\tau}(x) = \frac{\tau(x)-\tau_0}{\tau_0} = \frac{u_*(x)^2 - u_{*0}^2}{u_{*0}^2} = \left(A\frac{1}{\pi}\int_{-\infty}^{+\infty} \frac{\partial_\xi h(\xi)}{(x-\xi)}\mathrm{d}\xi + B\,\partial_x h(x) \right) \tag{7}$$

or equivalently in the Fourier space, where $\tilde{h}(k) = \int_{-\infty}^{+\infty} h(x)\exp(-\mathrm{i}kx)\,\mathrm{d}x$:

$$\tilde{\check{\tau}}(k) = \tilde{h}(k)\,(A|k| + \mathrm{i}Bk) \tag{8}$$

where τ_0 and u_{*0} are the unperturbed friction stress and velocity. A and B are both positive and weakly depend on the ratio L/z_0 [33–35]. The integral term is the solution to the slightly perturbed inviscid potential flow only. It is non-local, in phase

[1] Some may prefer the following explanation found in [6,31,32]. Well above the ground, the flow is inviscid and controlled by the balance between inertia and pressure gradient. As a result, the fluid velocity is in phase with the topography and maximum at the summit. In the inner layer, the turbulent stresses prevail on inertia and slow down the fluid. The inertia makes the fluid in the upper layers adapt with a delay. Hence, the bottom shear stress, as the fluid velocity in the inner layer, is maximum before the summit. This explanation is consistent, but the in-phase result of the inviscid, inertia-dominated flow ignores the inner layer.

with the topography and proportional to the bump aspect ratio H/L (height over length). The shear stress perturbation $\check{\tau}$ (Eq. (7)) is plotted in Fig. 1d–f for a Gaussian and a cosine topography profiles. As expected, a convex topography makes the flow accelerate, while a concave one makes it decelerate. The local term (on the right end) is proportional to the bump local slope and accounts for the bottom shear stress and velocity shift that is responsible for the bed instability. For bump length to roughness length ratio typically ranging between $5{\cdot}10^3$ and 10^5, A and B decrease when L/z_0 increases and typically range between $3.5 < A < 4$ and $1 < B < 2$ [35]. The calculation of the weakly perturbed potential flow leads to $A = 2$—and obviously $B = 0$. The phase shift between the topography and the bottom friction stress increases when the ratio B/A increases. The relative maximum increase of the bottom shear stress depends on the bump shape, is proportional to the bump aspect ratio and mainly depends on the A value. With the above-considered values for A and B, it is about $6.3 \times H/(2c)$ (resp. $6.3 \times 2H/\lambda$) for a Gaussian profile of amplitude H and RMS width c (resp. for a cosine of amplitude $H/2$ and wavelength λ). In practice, it is the maximum fractional speed-up ratio $\Delta S_{\max}$, which is measured:

$$\Delta S_{\max} = (u_{*\max} - u_{*0})/u_{*0} \simeq \beta H/L \tag{9}$$

In the limit of small perturbations, $\Delta S_{\max}$ is expected to be half the maximum shear stress increase ratio ($\tau \propto u_*^2$) so that β is expected to be about 3.1 (a dune is generally asymmetric so that the dune length L is almost the length from toe to summit). When measured close to the surface of the dunes ($H/L \sim 0.1$–0.15), $\Delta S_{\max}$ is reported to be larger and ranges between 0.4 and 1 [36–38,22]. Note that for dune aspect ratio, the perturbation is not small, but of order one.

2.2. Linear stability analysis

We now have all the ingredients to explain the genesis of dunes when wind blows over a sand bed. A perturbation of the flat surface perturbs the flow and the bottom shear stress, which reaches its maximum value before the top of the surface perturbation. Hence, the top can be a place where sand is deposited and a dune will grow. However, the actual sand flux is in spatial delay by a characteristic length l_{sat} with the shear stress and the corresponding value of the saturated sand flux. This length controls the wavelength of incipient dunes that grow from a flat sand bed and the minimal dune size (Fig. 1) [34]. The linear stability analysis has been done by Andreotti et al. [39] with the equations derived by Kroy et al. [34].

To do so, the sand bed is weakly perturbed by a cosine function:

$$h(x,t) = \Re[\hat{h}(x,t)],\ \hat{h}(x,t) = H_0 \exp[\mathrm{i}(kx - \omega t) + \sigma t] \tag{10}$$

where H_0, k, ω and σ are respectively the initial amplitude, the wave number, the angular frequency and the growth rate of the perturbation (all reals). The perturbation can propagate and will grow or flatten, depending on the sign of σ. Similarly, the perturbed sand flux reads:

$$\hat{q}(x,t) = q_0 \left(1 + \hat{Q}_0 \exp[\mathrm{i}(kx - \omega t) + \sigma t]\right) \tag{11}$$

where q_0 is the saturated sand flux value over the flat bottom and $\hat{Q}_0$ the dimensionless perturbation of the sand flux, which can be phase shifted (complex). The saturated sand flux derives from Eq. (7), assuming a simple power law between the saturated sand flux and the shear stress (neglecting the transport onset):

$$\hat{q}_{\text{sat}}(x,t) = q_0 \left[1 + (|k| A_{\text{q}} + \mathrm{i}k B_{\text{q}})\hat{h}\right] \tag{12}$$

where A_{q} and B_{q} are proportional to A and B, with a factor depending on the chosen power law. Here, we chose q_{sat} scaling like the bottom shear stress τ (and u_*^2), so that $A_{\text{q}} = A$ and $B_{\text{q}} = B$ (Eq. (7)). One sees already that A_{q} accounts for propagation (in phase) and B_{q} for growth (in phase quadrature). $\hat{h}$ and $\hat{q}$ are linked via the mass conservation: $\partial q/\partial x = -\partial h/\partial t$, which reads here:

$$(\mathrm{i}\omega - \sigma) H_0 = \mathrm{i}\, k\, \hat{Q}_0\, q_0 \tag{13}$$

Finally, the relaxation of $q(x)$ to the saturated value $q_{\text{sat}}(x)$ writes $\partial q/\partial x = (q_{\text{sat}} - q)/l_{\text{sat}}$ [34], which leads to:

$$\hat{Q}_0(1 + i\, k\, l_{\text{sat}}) = H_0(|k|\, A_{\text{q}} + \mathrm{i}\, k\, B_{\text{q}}) \tag{14}$$

Combining the equations of mass conservation (Eq. (13)) and sand flux relaxation (Eq. (14)), one finds:

$$\omega = \frac{q_0\, k\ |k|}{1 + k^2 l_{\text{sat}}^2}(A_{\text{q}} + B_{\text{q}}|k| l_{\text{sat}}) \text{ and } \sigma = \frac{q_0\, k^2}{1 + k^2\, l_{\text{sat}}^2}(B_{\text{q}} - A_{\text{q}}\, |k|\, l_{\text{sat}}) \tag{15}$$

σ is positive for a range of k values so that the perturbation of the sand bed (Eq. (10)) grows in height, i.e. the instability develops. This is true whatever the amplitude H_0 of the initial perturbation like for any linear instability. As expected, there is a minimum size for dunes, which flatten instead of growing ($\sigma < 0$) if $\lambda < 2\pi A_{\text{q}} l_{\text{sat}}/B_{\text{q}}$. The fastest growing mode ($\mathrm{d}\sigma/\mathrm{d}k = 0$) selects the elementary wavelength of incipient dunes: $\lambda_0 \simeq 3\pi A_{\text{q}} l_{\text{sat}}/B_{\text{q}}$. With $A_{\text{q}} = 4$, $B_{\text{q}} = 1.75$ (for $k z_0 \sim 10^{-4} - 10^{-5}$ [35]) and l_{sat} ranging between 0.5 and 1.2 m (i.e. for d ranging between 100 and 300 μm), the minimum

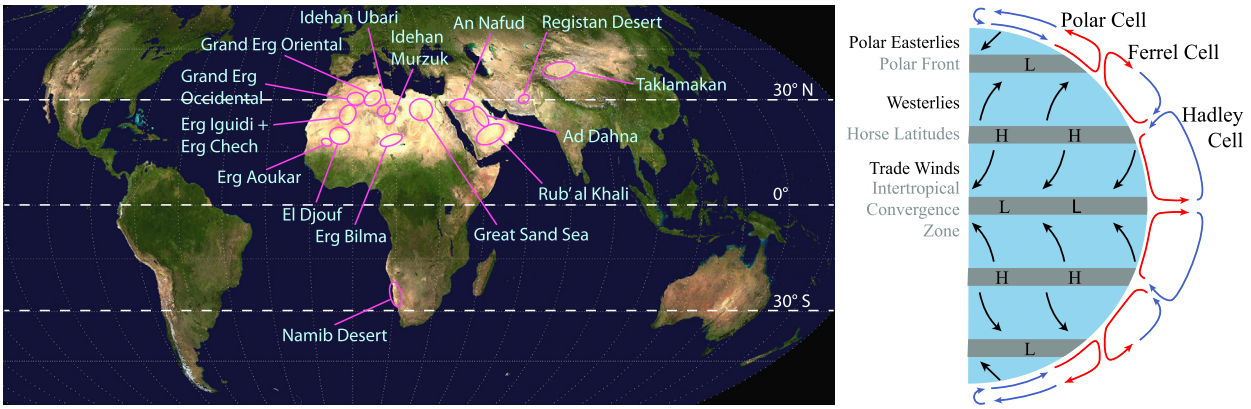

Fig. 2. (Color online.) Location of major active sand seas on Earth (Mollweide projection, planisphere from Wikipedia). Most of dunes in Australia are stabilized by the vegetation. Sketch of the circulation in the troposphere.

length for dunes ranges between 5.7 and 17 m and the initial—most-unstable—wavelength λ_0 ranges between 8.6 and 26 m, values that are consistent with the ones observed in the field ($\sim$ 6 to 10 m for the minimum dune size, $\sim$ 20 to 30 m for the initial wavelength [40,27]). Including the effect of the gravity through the dependence of the transport onset on the bed slope further stabilizes the small wavelengths (the transport onset increases with an increasing bed slope) [32]. Moreover, the inner layer thickness l_t decreases with a decreasing wavelength (Eq. (6)) so that for small wavelengths, the transport may take place in the outer layer, which should also prevent the instability. Nevertheless, the pertinent cut-off seems to be provided by the saturation length l_{sat}.

For large wavelengths, the velocity of incipient dunes is inversely proportional to their wavelength: $\mathrm{d}\omega/\mathrm{d}k \simeq 4\ \pi\ q_0\ A_q/\lambda$, which will be discussed later. As the saturation length imposes a significant minimum size for dunes, laboratory experiments on Aeolian dunes are difficult and one generally observes a vanishing pile [41]. The alternative to Aeolian dunes in laboratories are dunes underwater, where l_{sat} is about 1000 times smaller so that centimetric dunes are observed [19]. Then, if there is an obvious scale separation between ripples and dunes in the air, there is no such differentiation in water. In the following, we will often discuss the morphodynamics of dunes based on underwater experiments and numerical simulations. Note that l_{sat} underwater may not scale as the drag length $l_{drag} = d\,\rho_s/\rho_f$, since the transport may be of different nature (bed load) and because the settling limit velocity of grains is much smaller than the fluid flow velocity [42].

3. Sand seas location and wind regimes

Coastal dunes left apart, sand dunes on Earth are mainly observed in large systems called sand seas. These sand seas, also called Ergs, often correspond to structural basins where transported sand accumulate [43]. Most of them are localized in the arid regions of Horses latitudes ($\sim 30°$) where the heating dry air comes down at the junction of Hadley and Feller cells (Fig. 2). In these subtropical high-pressure belts, anticyclones form because of Coriolis effect and turn clockwise (resp. anti-clockwise) in the northern (resp. southern) hemisphere. As a result, winds are rather weak and distributed over a large range of directions, because of the moving character of anticyclones and the seasonal shift of the Hadley cell. From this belt, winds are going toward the poles or the equator and respectively deviate eastward (westerlies) and westward (trade winds) because of the Coriolis effect. Trade winds prevail when approaching the equator and it is worth noting that the sand path remarkably draws the trade wind pattern in the Sahara. This picture is locally modified by factors such as topography or proximity to the sea. One can also note that aridity is reinforced on western coasts of continents because air cools on contact with the cold water currents coming from the poles. There, anticyclones are especially stable and the Namibia and Western Sahara coasts are swept by semi-permanent anticyclones standing over the ocean, and undergo strong and mono-directional winds oriented towards the equator.

The shape of dunes depend on wind regimes and on the erodibility of the bed (non-erodible ground vs. erodible sand bed). They are usually classified into three groups, distinguished by the directional variability of winds [43]. This directional variability is classically depicted by the ratio between the resultant drift potential RDP (magnitude of the integrated sand flux vector) and the drift potential DP (sum of magnitudes of the individual sand flux vector). Hence, $RDP/DP = 1$ corresponds to unidirectional wind regimes and RDP/DP tends toward zero where winds are blowing in many different directions during a year. Where winds are unidirectional and sand is scarce, barchan dunes migrate on non-erodible floor (Fig. 3). As the amount of sand increases, barchans laterally link into barchanoid transverse dunes, which are perpendicular to the wind direction (Fig. 4). For a moderate wind direction variability ($RDP/DP \sim 0.5$), which is the dominant wind regime in Earth sand seas, linear dunes are observed (Fig. 5). Finally, sand seas exposed to a wide multidirectional wind regime ($RDP/DP \to 0$) show star dunes (Fig. 6).

4. The shape of dunes, their size and their orientation

In the linear regime (small dune height) of the instability, the height of dunes increases exponentially with time ($H(t) = H_0 \exp[\sigma t]$, Eq. (15)) with a constant wavelength (the most unstable wavelength λ_0). Their aspect ratio increases and at some point the wind boundary layer separates from the dune and a recirculation bubble forms (Fig. 3c). Above the inner layer, where the flow is driven by inertia and pressure gradients, the flow accelerates on the upwind positive slope and decelerates in the downwind side where the slope is negative. This imposes a positive pressure gradient (Bernoulli principle) in the downwind side of the dune that increases with a decreasing (negative) slope. This pressure gradient holds in the inner layer but is no more balanced by inertia. There, the fluid velocity is smaller than in the outer layer, reduced by the friction with the bottom, and this positive pressure gradient opposes the flow. When the slope of the topography in the downwind side is smaller than a given angle μ_b, the pressure gradient prevails on the turbulent input of momentum from the outer to the inner layer and the flow goes back up the slope. The inner layer detaches and a recirculation bubble forms. For a laminar flow over a dihedral, the critical angle μ_b is $-\pi/10$ [3], which seems to be the right order of magnitude observed in the field [30]. As a first approximation, the saturated sand flux drops to zero in the recirculation bubble. Progressively an avalanche face (also called slip face) at the repose angle ($\sim 30°$) appears on the downwind side of the growing and propagating dune. The dune converges towards an equilibrium shape.

4.1. Barchan dunes

Barchan dunes are “isolated” highly mobile dunes that propagate on a non-erodible rocky bed (Fig. 3). Their singularity, their relative small size and their recognizable shape make them the most documented ones. View from above, barchan dunes have a crescentic shape with two horns (also called arms) pointing in the downwind direction. Their windward side, called the stoss side, has a gentle slope of about 6 to 10°. The top of the dune is called the crest. The crest may or not correspond to the dune brink line, the sharp edge where the lee side begins and where the inner layer detaches to form a recirculation bubble, which reattaches downstream at a distance of 5 to 10 times the dune height [44,45]. The downwind side is also called the slip face or avalanche face since the slope is at the angle of repose ($\sim 30°$). Barchan’s height H, width W (distance between horns) and length L (from the tip of the stoss side to the foot of the avalanche face in the wind direction) are linearly (affine) related [46]. They are not self-similar objects but large barchans tend to constant aspect ratios H/L and H/W. Their height ranges from 1 to 50 m for a width and a length that range between 10 to 500 m. The aspect ratio H/L slightly increases with barchan size and typically ranges between 0.1 and 0.15 [46,47]. Large barchans exhibit a hierarchy of superimposed dunes that develop on their stoss side and arms (Fig. 3g) [40]. Because of the recirculation bubble, the avalanche face acts as a sand trap, and barchans can travel over long distances because they almost do not lose sand except from the tip of their horns. One can figure the barchan rolling like a caterpillar track, recycling its sand grains. The wind takes sand from the toe of the stoss side, leaves it at the brink where it falls down to the ground in an avalanche, to re-appear at the toe when the dune has propagated on its own length [48]. Barchan velocity typically ranges from 1 to 70 m/year [44] and depends on wind strength (saturated sand flux) and on barchan size. Within a same field, the velocity of barchans is inversely proportional to the dune height [1,44].

In order to understand their shape and propagating velocity, we first take these barchans for two-dimensional objects characterized by their central slice (Fig. 3b). Let us consider a sand pile sitting on a firm ground, initially almost flat and much longer than the saturation length l_{sat}. As it is evolving on a rocky floor with a weak incoming sand flux, the erosion at its foot is large—sand flux goes from zero to its saturated value on a length l_{sat}—and sand is deposited at the top, which makes the aspect ratio increase and the dune propagate. Then, a recirculation bubble forms at the brink and an avalanche face appears and progressively develops on the lee side. The aspect ratio (mean slope on the stoss side) cannot grow indefinitely in the presence of gravity. The increase of the transport onset with the bed slope could account for the saturation of the aspect ratio. However, as observed by Hesp and Hastings [46], such a small asymptotic aspect ratio ($H/L \sim 0.1$–0.15) should be set by aerodynamics.

On a theoretical point of view, Kroy et al. [34] proposed that the flow over the dune may still be described by Eq. (7), provided that the relief experienced by the wind is the stoss side of the dune, extended by the envelope of the recirculation bubble. Since the inner layer detaches for a topography angle smaller than μ_b, the envelope is modeled by a third-order polynomial function where the (negative) slope is never smaller than μ_b and smoothly connects to the dune brink and to the floor downwind. This strong assumption is *a posteriori* justified by the relevance of dune shapes this simulation code produces. Thus, the recirculation bubble length is set by the dune height H and μ_b and is proportional to H, which seems to be reasonable and consistent with the turbulent nature of the flow. Turbulent boundary layers over a flat semi-infinite plate grow linearly in height from the edge distance with a weak dependence on the Reynolds number [3]. Therefore, the length of the apparent topography experienced by the wind (stoss side of the dune extended by the recirculation bubble) increases with an increasing dune aspect ratio. As a result, the non-local term of the flow in Eq. (7) (i.e. the one with the prefactor A), which is in phase with the apparent topography, is in delay with the actual dune topography when the dune aspect ratio is large enough [39,34]. This effect leads to an erosion of the top of the dune. Then, the (numerical) barchan dunes always converge toward an equilibrium shape, which is reached when the sand flux is maximum at the top of the dune. Moreover, their aspect ratio saturates as the dune size increases. The parametric study of the barchan shape shows that the aspect

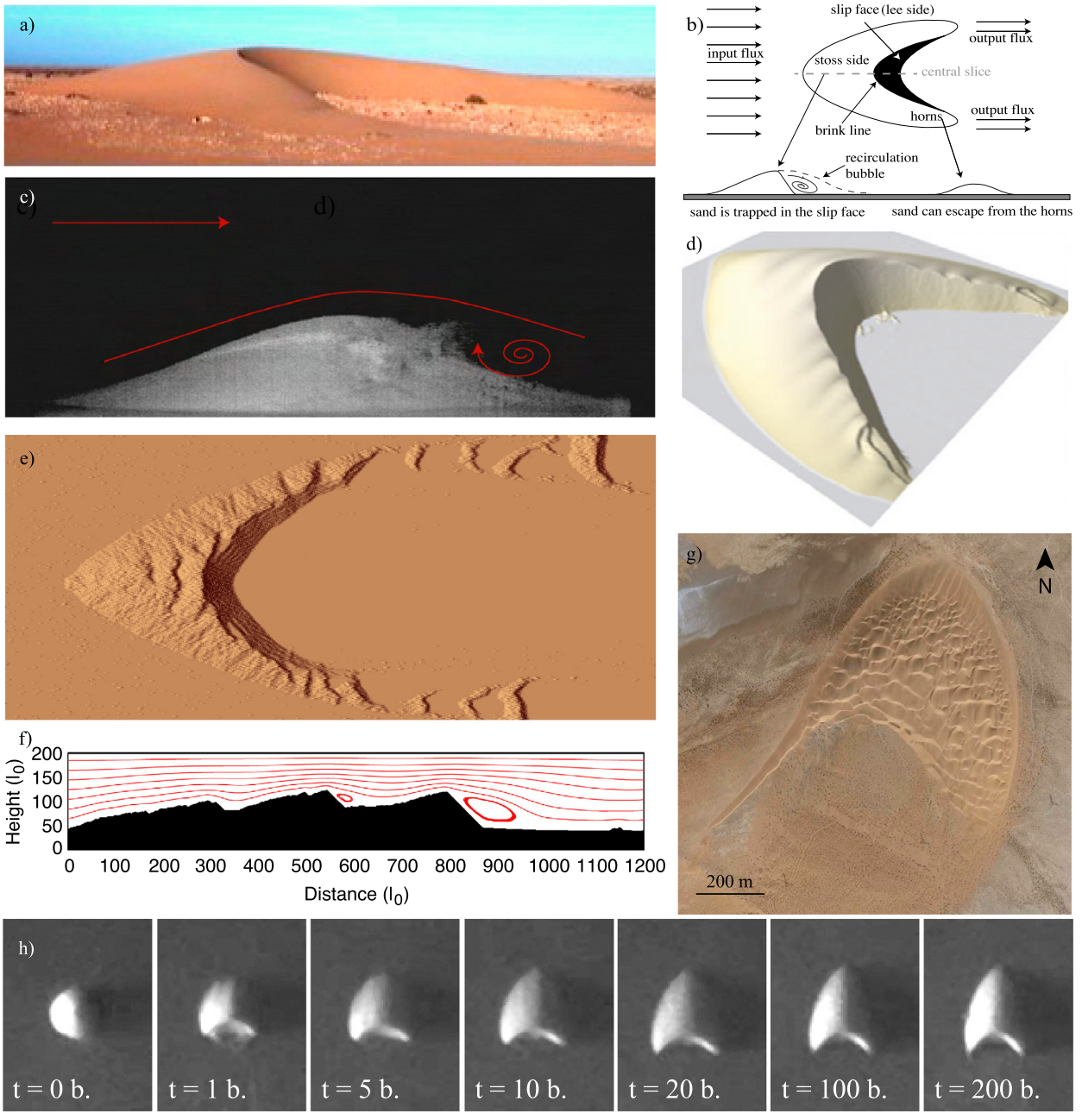

Fig. 3. (Color online.) a) Barchan dune close to Tarfaya in Morocco (credit: Pascal Hersen and Stéphane Douady). b) Sketch of a barchan, modified from [19]. c) Centimetric sand pile underwater. The flow goes from left to right and one observes grains going up the slope on the downwind side, i.e. a recirculation bubble has formed [24]. d) Numerical barchan (HerrDiff) [49]. e) Numerical barchan (ReScal) and (f) flow streamlines above it in the vertical plane of the barchan central slice [50]. g) Mega barchan (Ω1) in Morocco (from Google Earth). h) A barchan forms from a sand pile in underwater experiments. It is 2 cm wide.

ratio increases when B increases or A decreases [51]. This is expected since B is the factor of the destabilizing term and because the shift between the maximum shear stress and the maximum of topography increases when B/A increases [51].

Fourrière et al. have carried out the calculation of the perturbed flow (Eq. (7)) over a sinusoidal bottom: $h(x) = (H/2)\sin(kx)$ (dune height H is two times the sine amplitude) including the first-order non-linear correction. This correction is proportional to $(kH/2)^3$—for symmetry reasons: a bump is the opposite of a trough—and they found it to be negative for the local term (i.e. the one with a prefactor B) responsible for the phase shift [35,52]. Following Eq. (8), the local term is proportional to $B(kH/2) + B_3(kH/2)^3$, where B_3 is the coefficient of the non-linear correction. The topography-flow phase shift vanishes and the dune aspect ratio saturates when $kH/2 = \sqrt{-B/B_3}$ [52]. For typical roughness to wavelength ratios kz_0 ranging between 10^{-4} and 10^{-5}, they found $B \simeq 1.75$ and $B_3 \simeq -40$, which also gives a reasonable value for the

equilibrium aspect ratio: $H/\lambda \simeq 6.7 \cdot 10^{-2}$ [31]. Note that in these calculations, as for the linear calculation of Eq. (7), the shear stress can be negative (opposite to the flow) if the dune aspect ratio and the coefficients A and B are large enough. Although the vanishing of the shear stress signifies the detachment of the boundary layer, the recirculation bubble affects the outer flow, which appears to be inconsistent with the assumptions made for the calculations.

Since the first 2D barchan dunes of Kroy et al. [34], the simulation code of this team has significantly improved, taking into account the 3D perturbation of the flow [49]. The simulated dunes closely correspond to field observations, at least as long as isolated dunes are considered (Fig. 3d). A more precise model of the recirculation bubble seems to be required to simulate closely-spaced dunes [53] or to generate fully-developed superimposed dunes on the stoss side of large barchans (Fig. 3g). These features are reproduced by an alternative numerical model, which is not based on differential equations, but couples a cellular automaton of sediment transport with a lattice-gas cellular automaton for high Reynolds-flow simulation [26,54]. The flow is computed in 2D vertical planes but the transport of grains is in 3D. In this approach, although the Reynolds number is moderate, flow features like the recirculation bubble and back flows are present without being phenomenologically included (Fig. 3e–f). Phenomenological inputs remain though in the discrete set of transition that simulates sediment transport. Contrary to the approach of Kroy et al., it does not provide a set of equations for theoretical work. However, this counterpart is balanced by features like the access of the sedimentary structuration of the sand bed (Fig. 5). In the following, we will refer to this model as (ReScal) and to the ones based on differential equations as (HerrDiff).

Underwater experiments [55] and ReScal-numerical simulations [56] have shown that the aspect ratio of barchan dunes increases with flow velocity. This is consistent with the non-linearity of the saturated sand flux because of the transport onset (e.g. Eq. (5)). When the unperturbed velocity u_{*0} is close to the transport onset velocity u_d (i.e. $u_{*0}^2 \propto u_\mathrm{d}^2(1+\epsilon)$ with $\epsilon \ll 1$), the ratio between the saturated sand flux at the top ($\propto u_{*0}^2[1+2\beta H/L] - u_\mathrm{d}^2$, Eqs. (9) and (5)) and the one at the toe ($\propto u_{*0}^2 - u_\mathrm{d}^2$) increases drastically (scales like $2\beta(H/L)/\epsilon$). This leads to an increase in the sediment transport at the top compared to the one at the toe, when the flow velocity decreases towards the transport onset velocity, and consequently to a decreasing aspect ratio (i.e. elongated barchans).

Barchan dunes propagate at a velocity inversely proportional to their height, which directly follows from mass conservation [1]. For a 2D barchan propagating in the x direction, the mass conservation reads $\partial q/\partial x = -\partial h/\partial t$. If the dune propagates with a stationary shape: $\partial h/\partial t = -c\ \partial h/\partial x$, where c is the barchan velocity, and $c = [q(x) - q_\mathrm{in}]/h(x)$, where q_in is the incoming sand flux, which can generally be neglected. To the first order in dune aspect ratio H/L, the maximum saturated sand flux is $q_\mathrm{M} = q_0(1+2\beta H/L)$ ($\beta H/L = \Delta S_\mathrm{max}$, Eq. (9)). As before, the factor of two comes from the linearization of the transport law ($q \propto u_*^2$, Eq. (5)) where the transport onset has been neglected. For large barchans, the aspect ratio H/L can be considered constant. Then, dunes propagate at a velocity that is inversely proportional to their height: $c = [q_0(1+2\Delta S_\mathrm{max})]/H$ [1], where ΔS_max is constant for large dunes with a reported value of about 1 [29,36,45,37,40,57,22]. However, considering the whole size range of barchan dunes, their velocity is better described by a relation such as:

$$c = a\, q_0/(H + H_0) \tag{16}$$

with $a \simeq 3$, which is a smooth cross-over between the above velocity for large dunes and a finite value for dunes of vanishing amplitudes [40]. These small dunes cannot be considered scale-invariant. At the minimum length L_min set by l_sat, they turn into flattening piles without slip face called domes. For $H = 0$, one expects $c \propto q_0/L_\mathrm{min}$, which is also the scaling of the velocity of incipient dunes on a sand bed (Eq. (15)). In the western Sahara where coastal winds are strong compared to continental deserts, the saturated sand flux q_0 is about 67 m^2/year,[2] so that a 4.4-m-high barchan travels a distance comparable to its length ($\sim$ 45 m) in a year time. This characteristic time t_to for a dune to propagate over a distance that is equal to its length ($t_\mathrm{to} = L/c$) is called the turnover time. It is the characteristic time for a dune to adapt to a change in wind regime [1,59]. It is particularly important in regions where the wind blows in different directions during the year (or over a longer period time). Indeed, depending on their size and the corresponding turnover time, dune shape and stratigraphy adapt and result from the current wind regime (small dune) or integrate and keep the memory of the variable wind regime over a longer time (larger dunes).

The 3D shape of a barchan can easily be understood looking at the formation of a subaqueous barchan from an initial conical pile (Fig. 3). As we previously saw, wind erosion on the back of the sand pile leads to the formation of a crest perpendicular to the wind direction and to the formation of a slip face. According to mass conservation, the thin sides of the pile propagate faster (H is smaller) than the central slice, which turns the pile into a crescentic shape with elongated arms. Because of gravity and wind deflection, a part of the sand flux on the stoss side is redirected towards the barchan sides and the two horns. This incoming sand flux slows down the propagation of the horns. As the arms outstrip the central body, the lateral aspect ratio increases, which increases the deflection of the sand flux towards the barchan horns and slows down their propagation even more. The barchan stops elongating and migrates as a whole in a dynamical equilibrium shape when the sand redirection towards the horns is just enough to slow them down to the velocity of the central body [19]. Note that the barchan horns are devoid of avalanche face so that (little) sand escapes from them.

[2] This value is derived from the assimilation of wind data provided by the ERA-Interim reanalysis over the last 35 years [58]. Local measurements of the wind velocity over the year 1999 give 81 m^2/year [40].

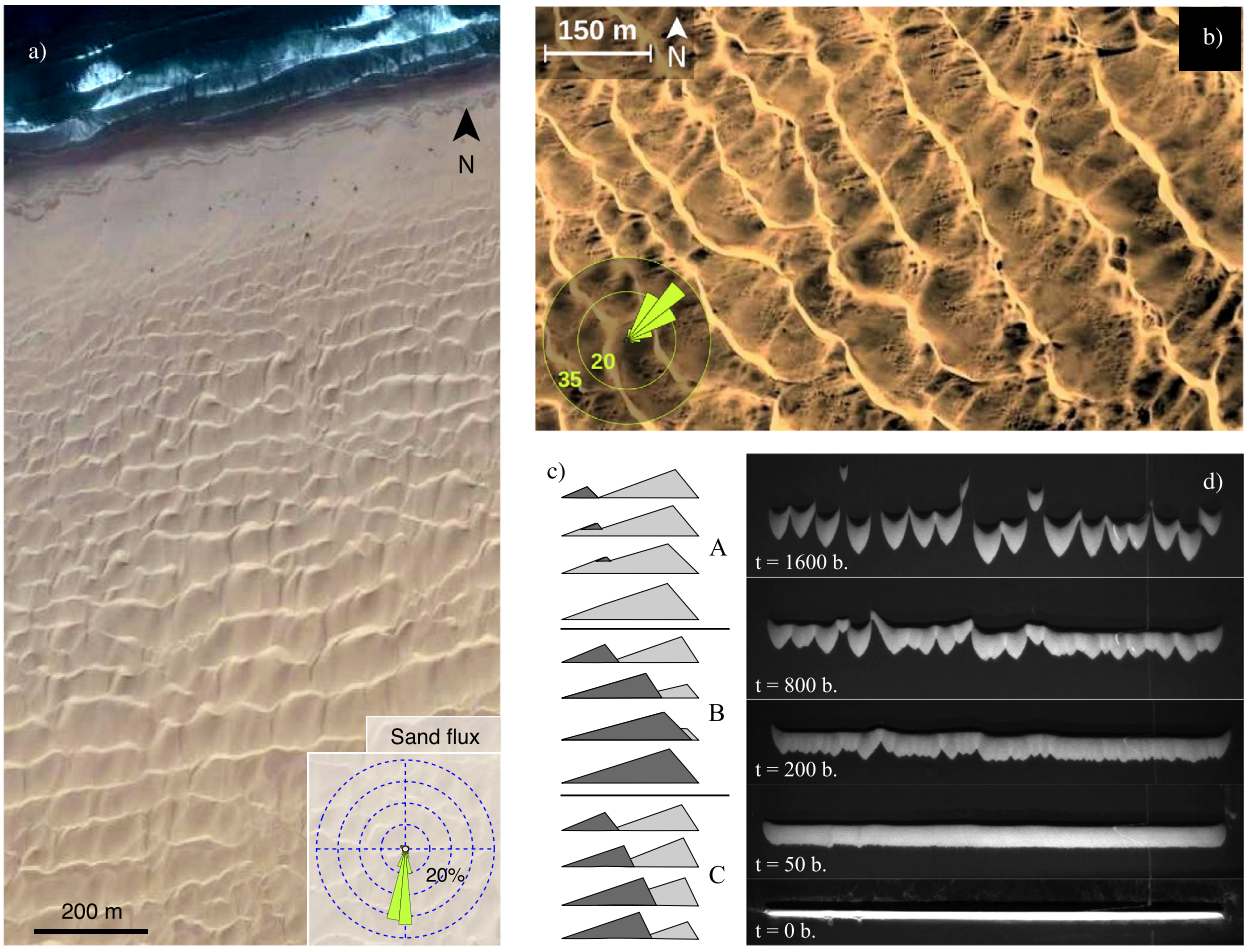

Fig. 4. (Color online.) a) Transverse dune in Morocco (28.05°N, −12.26°E, from Google Earth) The sand flux rose is calculated with wind data from the ERA-Interim assimilation data base [58] using the sand transport law (Eq. (5)) with $u_d = 0.2\ \mathrm{m\,s^{-1}}$. The sand flux is pointing towards the outside of the rose. This stands for all sand roses. $RDP/DP \simeq 0.84$. b) Transverse dune in the Moçâmedes desert in Angola (16.53°S, 12°E, from Google Earth). $RDP/DP \simeq 0.88$. c) Amalgamation processes (see text). The flow is directed towards the right. d) A subaqueous isolated transverse dune breaks into barchans while propagating. The flow is directed towards the top of the pictures.

4.2. Transverse dunes

Transverse dunes are observed in deserts where the wind is unidirectional and where the bed is not a firm ground but an erodible sand bed (Fig. 4). They are long linear sinuous (crescentic) ridges with a crest that is perpendicular to the wind. Their aspect ratios and heights are comparable to the ones of barchans. Parteli et al. measured an aspect ratio H/L ranging between 0.07 and 0.13 for six dunes of height H ranging between 7 and 10 m [53]. The main difference with barchans is that transverse dunes are closely spaced and arranged in a field with a well-defined wavelength. This wavelength is generally significantly larger than the one of incipient dunes ($\lambda_0 \sim 20$ to 30 m), which is found for superimposed patterns on the stoss side of big dunes. Therefore, once transverse dunes are formed, their wavelength shall evolve through time and may saturate at some point.

After the linear regime, during which the amplitude increases exponentially with time and the wavelength remains constant, underwater experiments show that the wavelength slowly increases with time [23,35,25,60]. The slight differences in height between dunes leads to slight differences in propagation velocity ($c \propto 1/H$) and, as a result of this dispersive behavior, transverse dunes collide and interact. Three different longitudinal interactions have been identified [23,61] as shown in Fig. 4c: (A) the upstream dune propagates on the downwind one, decreases in size and deposits its sand on the stoss slope of the impacted dune, which leads to the merging of the two dunes into a larger one, (B) the upstream dune grows while approaching the top of the impacted dunes and screens it with its recirculation bubble so that the two merge, (C) the two dunes collide and exchange mass but do not merge (through passing dunes). The interaction (B) is generally recognized as the prevailing one [23,62,63]. In water experiments, the wavelength seems to increase linearly with time [23,25,35] when the particle Reynolds number Re_p (i.e. calculated with the grain size) is large and logarithmically with time when Re_p is small (the transition occurs around $Re_p \sim 4$ [25]). Small particles may lie in the viscous boundary layer.

Although the spatial evolution of a dune field may be equivalent to a temporal one (Fig. 4a), field observations are limited. Nonetheless, in December 2007, a parcel of the Tenger desert in China was flattened (37.56°N, 105.03°E) and the evolution of the dune field has been followed [27]. Between early 2008 and late 2011, the amplitude increased up to 2.5 m and the wavelength remained constant ($\sim$ 25 m). The aspect ratio has reached a value comparable to the one of non-flattened mature dunes in the vicinity, which are four to five times longer. Hence, dune interactions may now be at work and recorded. However, the wind regime there is multidirectional.

On a theoretical point of view, the increase of the wavelength with time, which is called a coarsening process, arises from the non-linearities of the equations that describe the dynamics of the system. Theoretical 2D studies of dunes in a laminar flow show a coarsening, which never stops, where the wavelength λ increases almost linearly with time (between $t^{0.8}$ and t [62,64]). The coarsening in these studies is ascribed to the non-linearity of the transport onset, which also depends on the bed slope. It should be noted though that the dynamics and aspect ratio of these dunes in the laminar, viscous regime, seem different from what is observed in Nature and in underwater experiments. In these models, the aspect ratio of dunes decreases with time and the increasing wavelength, whereas the aspect ratio seems to be roughly constant in underwater experiments when $Re_p > 4$ and to slightly increase with dune length in Nature, at least for barchans [46]. Recently, numerical simulations (ReScal) of transverse dunes have shown a coarsening process where $\lambda \propto t^{0.3}$, which interestingly stops at some point for aerodynamical reasons: the shear stress in the trough falls under the transport threshold. The non-linearities are many and the scenario is still unclear. The recirculation bubble and the 3D outer flow are believed to play a major role here and great efforts are made to characterize the flow [37,65,66,57]. The wavelength of Earth deserts sand dunes may also be stabilized to a maximum length set by the depth of the outer flow [52], which will be addressed later.

Transverse dunes are not perfect ridges along their lateral dimension too, their crest is sinuous (Fig. 4). Experiments [67] and numerical simulations (HerrDiff [68,69]) have shown than an isolated transverse dune is unstable when propagating on a non-erodible ground and without input flux. A perturbation in height or length leads to a perturbation in the propagating velocity which amplifies (Fig. 4d). The redirection of sand flux on the stoss side, from the longer and higher slices towards their neighboring slices of smaller amplitude and length, is not enough to stabilize the perturbation. The perturbation even amplifies as the sand in the concave avalanche face is redirected towards the center, i.e. the longest and highest slice.[3] Thus, on the characteristic turnover time to propagate over a distance comparable to its length, the transverse dune laterally destabilizes into a tray of barchans, whose size is set by the height of the initial transverse dune [68]. Indeed, the barchan is exactly the equilibrium shape for which lateral flux on the stoss side balances velocity differences of adjacent slices. Obviously, this mechanism is also at play for a field of transverse dunes, which are sometimes referred to as barchanoid ridges.

4.3. Linear dunes, their orientation in multidirectional wind regimes

With multidirectional wind regimes arises the question of dune orientation. Under the action of a mono-directional wind, a sand bed destabilizes and show crests that are perpendicular to the wind's direction, which is also the propagation direction of the dune. In a multidirectional wind regime with winds blowing with different strengths and directions as a function of time, each individual wind contributes to the development of dunes. Thus, if large enough, dunes integrate all contributions and show an averaged crest orientation that maximizes the sand transport normal to the dune crest (Fig. 5), as shown first by the experiments of Rubin and Hunter [70] and by others thereafter [71,67,72,60,27].

Let us consider a field of linear dunes of height H, length L (wavelength) and crest line orientation α in the standard basis $(\vec{i}, \vec{j})$ shaped by an arbitrary wind cycle of duration T. The magnitude q_0 and the direction θ of the unperturbed saturated sand flux depend on time t. Thus, the maximum saturated sand flux close to the crest can write:

$$\vec{q}_{\max}(t) = q_0(t)\left(1 + 2\ \beta\ \frac{H}{L}\,|\sin[\theta(t) - \alpha]|\right)\left[\cos\theta(t)\,\vec{i} + \sin\theta(t)\,\vec{j}\right] \tag{17}$$

where $\beta\frac{H}{L}\,|\sin[\theta(t) - \alpha]|$ is the speed-up ratio $\Delta S_{\max}$ (Eq. (9)), where the dune aspect ratio is the one experienced by the wind [56,60]. As done previously for the barchan velocity, the factor two comes from the linearization of the transport law ($q_{\text{sat}} \propto u_*^2$, Eq. (5)), where the transport onset has been neglected. Over a period time T, the average magnitude and direction of the sand flux at the dune crest is then a function of the dune's orientation α:

$$\vec{Q}_T = \frac{1}{T}\int_T \vec{q}_{\max}(t)\,\mathrm{d}t \tag{18}$$

From the conservation of mass $\vec{\nabla}\cdot\vec{q} = -\partial h/\partial t$, one can derive a characteristic growth rate:

$$\sigma(t) = \frac{1}{H}\frac{\partial H}{\partial t} \propto \frac{q_{\max}(t) - 0}{HL/\,|\sin[\theta(t) - \alpha]\,|} \tag{19}$$

[3] However, the secondary fluid flow on the lee side opposes the redirection imposed by gravity.

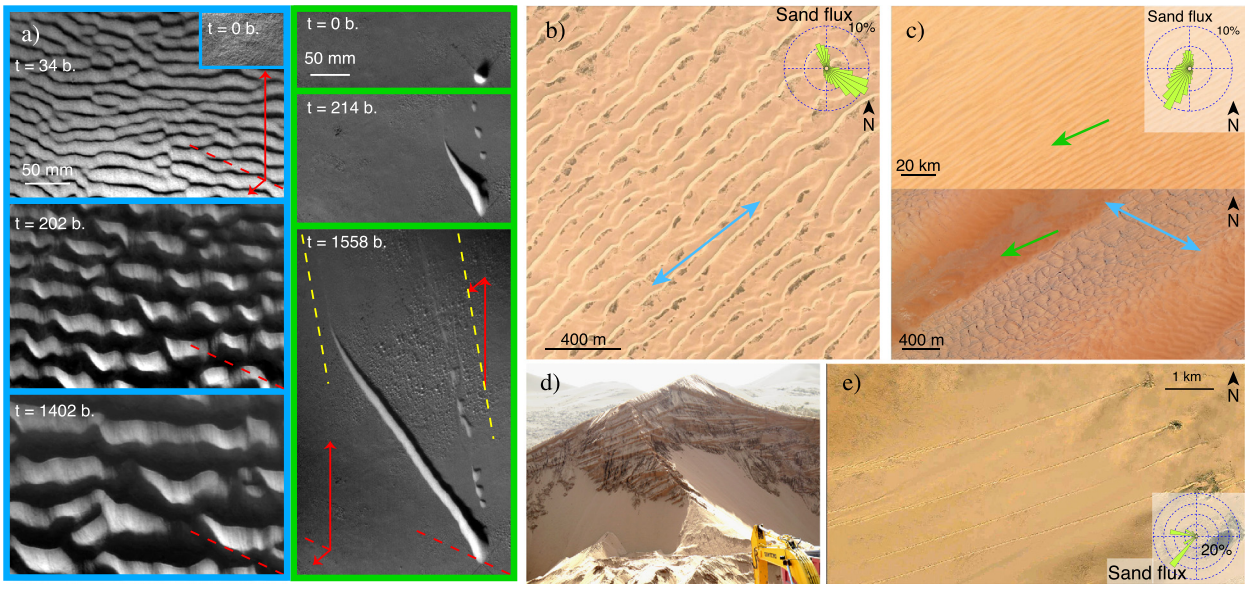

Fig. 5. (Color online.) a) Linear dunes under water growing from a sand bed (blue) or a localized sand source (green) under the same bimodal flow (red arrows). Yellow dashed line show the direction of the unperturbed resultant direction [60]. b) Oblique dunes in Mu Us Desert (China, 38.8°N, 107.7°E, from Google Earth), $RDP/DP = 0.44 \pm 0.04$. c) Linear dune field (top) and superimposed bedform (bottom) in Rub' al Khali (Saudi Arabia, 19.3°N, 48.5°E, from Google Earth), $RDP/DP = 0.46 \pm 0.04$. Sand flux in (b) and (c) is calculated with wind data from the ERA-Interim project [58]. Green and blue arrows are the prediction for the orientation of finger dunes (α_F) and dunes growing from a sand bed (α_I), obtained with Eqs. (20) and (17) using the shown sand flux roses [60]. d) Stratification of an oblique dune in the Tengger desert. The sedimentary structure is a record of the dune dynamics (http://walrus.wr.usgs.gov/seds/). e) Seif dunes extending from topographic obstacles in Niger (18.75°N, 12.58°E). The sand flux rose is calculated with wind data of the airport weather station in Bilma, Niger, between 2000 and 2013 (18.68°N, 12.92°E). $RDP/DP \simeq 0.73$. [63].

Here, dunes with an avalanche face rather than incipient dunes are considered, so that the characteristic variation of the sand flux is $(q_{\max} - 0)$ rather than $(q_{\max} - q_0)$. The sand flux varies on a characteristic length, which is the dune length experienced by the wind. Thus, if dunes are large enough with a turnover time much longer than T, the mean growth rate σ_T scales like [60]:

$$\sigma_T \propto \frac{1}{THL} \int_T q_{\max}(t)\, |\sin(\theta(t) - \alpha)|\, \mathrm{d}t \tag{20}$$

where the aspect ratio of the dune has been considered constant over the time period T. σ_T depends on the angle between the wind direction and the dune crest orientation through the apparent aspect ratio both in $q_{\max}$ (Eq. (17)) and in the characteristic length for flux variation. Besides, it takes equally the contributions of winds with opposite directions, which both contribute to build up the dune. In the development of the bed instability, the preferred dune crest orientation α_I is the one with the highest growth rate σ_I, such that $\mathrm{d}\sigma_T/\mathrm{d}\alpha = 0$. Depending on wind regimes, dunes will either be perpendicular (transverse dunes, typically for acute distributions of wind directions), oblique or parallel (longitudinal dunes, typically for obtuse distribution of wind directions) to the resultant wind direction [70,71,67,72,60]. As a result, transverse dunes migrate (i.e. propagate in a direction perpendicular to the dune crest), longitudinal dunes extend (in the crest direction), and oblique dunes both migrate and extend. We noted that the sinuosity of the crest of transverse dunes results from their migration. Hence, linear dunes should show even straighter crest lines as they are aligned with the resultant sand transport direction and their migration is limited [73]. Moreover, a sand flux parallel to the crest further stabilizes the integrity of the dune crest line [67,73].

In Eq. (20), the aspect ratio and the dune orientation are considered constant over the wind regime time period T (typically a year on Earth), which is a strong simplification. Moreover, one can question the scenario of the development of the bed instability for mature dunes, which interact and collide. Nevertheless, the orientation of dunes on erodible sand beds in underwater experiments [71,67,60] and in Earth deserts [60,27] compare well to these predictions. The scenario of dune coarsening through dune propagation and collision was investigated, looking at the dune orientation that would be perpendicular to the propagation direction, i.e. transverse dune, perpendicular to the sediment flux Eq. (18) [60]. This scenario fails to reproduce experimental data [60].

The orientation inherited from the bed instability scenario holds for dunes on an erodible sand bed. But the crest line orientation is different when dunes are growing on a non-erodible ground from a localized sand source [60]. In such a case, underwater experiments [60] and numerical simulations (ReScal [63]) with an obtuse bimodal flow regime showed that a straight finger dune extends from the source, with a sharp crest and a reversing avalanche face (Fig. 5a). The very growth mode of this finger dune makes it aligned with the mean sand transport direction, which is different from the

mean unperturbed flow direction because of the interaction between dune topography and sand flux (Fig. 5). Thus, a same multidirectional flow regime can lead to two different dune orientations, depending on the overriding mechanism for the formation of dunes, i.e. increasing in height from the destabilization of a sand bed or elongating in a finger on a non-erodible ground from a localized sand source [60].

The dune orientation in numerical simulation is well predicted by Eqs. (17) and (18), assuming a constant aspect ratio with a reasonable speed-up value $\beta H/L = 1$ [63]. The crest line orientation α_F of finger dunes is such that the mean sand flux (Eq. (18)) is aligned with the crest line of the dune. Eq. (18) gives the right trend, but fails to quantitatively predict the orientation of finger dunes in underwater experiments. This discrepancy may be ascribed to secondary flows in experiments (in ReScal simulations, the flow is computed in 2D vertical planes). When the flow makes an angle with the dune trend, the flow is deflected. The streamlines tend first to cross the crest line perpendicularly. Then, on the lee side, the recirculation bubble forms a helical vortex that goes along the dune [38]. These redirections can be qualitatively understood through Bernoulli's principle, when considering that velocity is maximum and pressure is minimum at the dune crest. Pressure gradients then tend to redirect the flow as described. In the field, this mechanism has been recognized to actively transport grains along dunes when the wind blows obliquely [74]. However, this effect appears to be incidental in underwater experiments. In experiments, the finger dune cross-sectional shape constantly adapts to the wind. In particular, the avalanche face flips from one side to the other. When the flow direction changes, the sand flux is much larger when the fluid flows frontally over the avalanche face than later when the dune shape has adapted to the flow. The discrepancy between experiments and Eq. (18) shall be ascribed to the non-constant aspect ratio in experiments [60].

When the inter-dune area is free of sand, the orientation of many linear dunes in the field are well predicted by Eqs. (17) and (18) using the wind data provided by the ERA-Interim reanalysis from 1979 to nowadays (Fig. 5) [58,60]. These 35 years are short compared to the turnover time of most linear dunes in the field. The prediction of dune orientation in the field is less sensitive to the hypothesis of a constant shape because the wind direction changes less abruptly than in experiments and is widely distributed. For the same reason, the chosen value of the speed-up $\beta H/L$ has also little influence on the prediction of dune orientation in the field [60]. Finger dunes have a longitudinal orientation in nature and many longitudinal dunes on Earth have been recognized to extend in the mean resultant direction [74–76]. For given wind regimes, the longitudinal orientation could also correspond to the orientation of dunes growing from a sand bed. However the two orientations α_F, corresponding to the mean sand flux for finger dunes, and α_I, corresponding to the maximum growth rate σ_I for sand bed dunes, are usually distinct for the multidirectional wind regimes of Earth sand seas (Fig. 5).

Longitudinal dunes without sand in the inter-dune areas are the most common dunes in Sahara sand seas, probably because they are finger dunes extending away from geomorphologic sand sources (e.g., coastal or fluvial–alluvial systems). These dunes are arranged in parallel ridges, with a well defined wavelength when they are large. The large ones may be hundreds-of-kilometers-long (along crest direction) and up to 200 m high, with superimposed dunes on their back, whose orientation is usually oblique or transverse to the primary longitudinal dune trend (Fig. 5) [77,43]. The coexistence of dunes or bedforms with different orientations and scales is sometimes interpreted as the signature of a temporal change in the wind regime, because to different dune scales correspond different turnover times [43]. However, the huge longitudinal dunes, like any large dune, represent an erodible floor where the bed instability develops. The smaller longitudinal dunes on rocky floor do not generally exhibit a characteristic wavelength. Being thin in cross section with a sharp slightly sinuous crest line, they are often called seif dunes, which means sword in arabic. The term seif dune is sometimes also used for dunes that occur on an erodible floor. These seif dunes often nucleate after topographic obstacles where sand accumulates (Fig. 5e). Asymmetric barchan dunes in multimodal flow regimes often exhibit an elongated horn in the mean transport direction, as observed in the field [1,78,79] in underwater experiments [67,80] and in numerical simulations (HerrDiff [81], ReScal [63]). This elongated horns are reminiscent of incipient seif dunes [1,78].

The stability of a finger dune aligned in the mean sand flux direction may surprise. Indeed, such a dune cannot develop under a unidirectional wind or more generally when there is a strong prevailing wind direction. In a multimodal wind regime, the finger dune pointing in the mean sand flux direction is blown on either side by winds, which can build and sustain the aspect ratio of the dune. One can thus construct an equivalent growth rate σ_F (Eq. (20)) for the finger dune orientation α_F, which is by definition smaller than the maximum growth rate σ_I for dunes that would be oriented in the bed instability mode with an orientation α_I [60]. The phase diagram of finger dunes extending from a localized sand source in bimodal wind regimes (i.e. varying the angle θ and the transport ratio N between winds) has been numerically investigated by Gao et al. (ReScal) [63]. When the angle between winds is too acute (typically θ smaller than 70°) or the transport ratio is too large (typically N larger than 4), the finger dune growing from a sand source is unstable and asymmetric barchans form. The transition between finger dunes and barchans is fairly well captured by the ratio σ_F/σ_I (finger dunes are observed when $\sigma_F/\sigma_I > 0.4 \pm 0.1$) both in the simulations (ReScal) and in a dune field around the Tibetsi massif of East Central Sahara [63]. Taniguchi et al. (under water experiments, [80]) and Parteli et al. (numerical simulations, HerrDiff, [81]) have investigated the corresponding phase diagram for asymmetric barchan dunes, starting from a conical pile, and looking at the pair (θ, N) for which a horn elongates in the mean transport direction. Their results with this slightly different limit condition are similar except that no horn elongates when θ is smaller than 90°. Moreover, the propagation of the barchan body, which stands for the source, modifies the elongation direction of the horn.

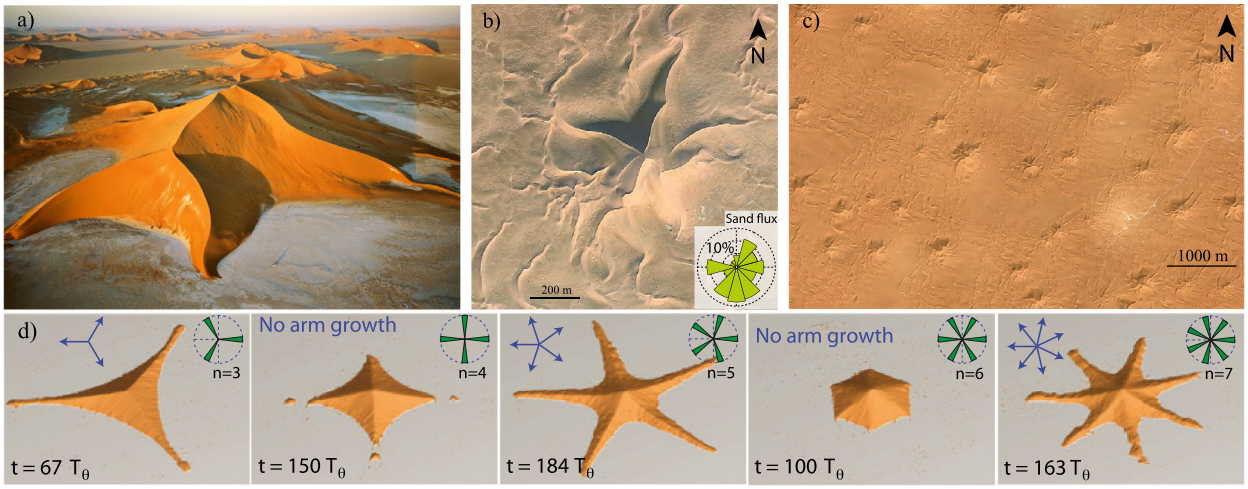

Fig. 6. (Color online.) a) Star dune in Rub-al-khali, courtesy of ©George Steinmetz. George Steinmetz takes beautiful aerial landscape pictures seated in a paraglider (http://www.georgesteinmetz.com). b) c) Star dunes in Algeria (b: 30.87°N, 7.9°E, c: 31.22°N, 7.89°E, from Google Earth). Sand rose is calculated with the Hassi-Messaoud airport wind data from 2005 to 2009. $RDP/DP \simeq 0.18$. d) Star dune from numerical modeling (ReScal) [56].

4.4. Star dunes

Star dunes are the largest aeolian dune patterns in Earth's sand seas [82]. They occur in regions with a wide multidirectional wind regime so that the overall resultant sand flux is small. Thus, they are usually observed at the high-pressure belts latitudes [83]. Sitting on a non-erodible floor, they exhibit an overall pyramidal shape with interlaced arms (Fig. 6). They are about 100 m high and 1 km wide. Only large dunes can integrate a highly-variable wind regime. Like other massive dunes, they integrate winds over a long time scale and show a hierarchy of superimposed bedforms starting at the elementary length scale ($\sim$ 20 to 30 m). Within the field, they draw a regular network and seem to interact through their radiating arms (Fig. 6c).

Zhang et al. have run simulations (ReScal, [54]) looking at the evolution of an initial truncated conical pile sitting on non-erodible ground and subject to a symmetric flow regime with n distinct directions, with n ranging from 3 to 7 [84]. The flow periodically changes between the regularly spaced n directions ($\theta_p = 2p\pi/n,\ p \in [1, n]$) and the flow strength and time duration T_θ in each direction are the same, so that the mean flux of sediment is zero. The symmetry of the flow regime is recovered in the shape of the emerging star dunes (Fig. 6d). When the number n of wind directions is odd, n arms elongate from the central pile against the individual wind directions. The elongating arms reach a stationary state characterized by constant width, height and elongation velocity, which are controlled by the time duration T_θ in each wind direction. When n is even, no arm elongates [84]. In these simulations, star dune arms appear to be finger dunes, which elongate from the massive pyramidal center of the star dune.

These results are another demonstration of the interaction between the dune topography and the sediment transport. The direction of arms' elongation are predicted when considering the speed-up effect as in Eq. (17) [84,60]. Although the resultant sand flux is zero on a flat bed, when the number n of winds is odd, the speed-up (Eqs. (18) and (17)) selects n elongation directions for which the dune line crest orientation and the resultant sand flux direction match. Arms are found to elongate against each individual wind direction. It is worth noting that the speed-up vanishes when wind and crest line are aligned because the apparent aspect ratio of the dune vanishes (Eq. (17)). For an even number of wind directions, there is not such a selection and no arm elongates.

In these simulations (ReScal) the flow is described by the interactions of discrete gas cells, which collide and exchange momentum. The boundary conditions in the longitudinal direction of the flow are periodic, but it is necessary to bound the flow in the transverse direction, otherwise the density of gas particles would rapidly vanish with time. Thus, the flow has a finite depth and is bounded in the upper limit by a roof where a perfect slip condition applies [26,54]. In the particular flow regime used to study star dunes, the overall resultant sand flux is zero. Thus, sand initially accumulates and aggregates in the center pile of the dune, which grows. It is only once this pile has reached a maximum height and length imposed by the depth of the flow that arms start to elongate [56]. Because of the confinement of the flow along the vertical axis, the sand transport at the top of the dune increases rapidly with dune length, once the dune length (and height) is comparable to the flow depth. This stops the growing process of the center pile and allows arms to elongate. Such symmetric wind regimes do not occur in Nature but the flow depth seems to similarly control the size of these giant dunes on Earth [52].

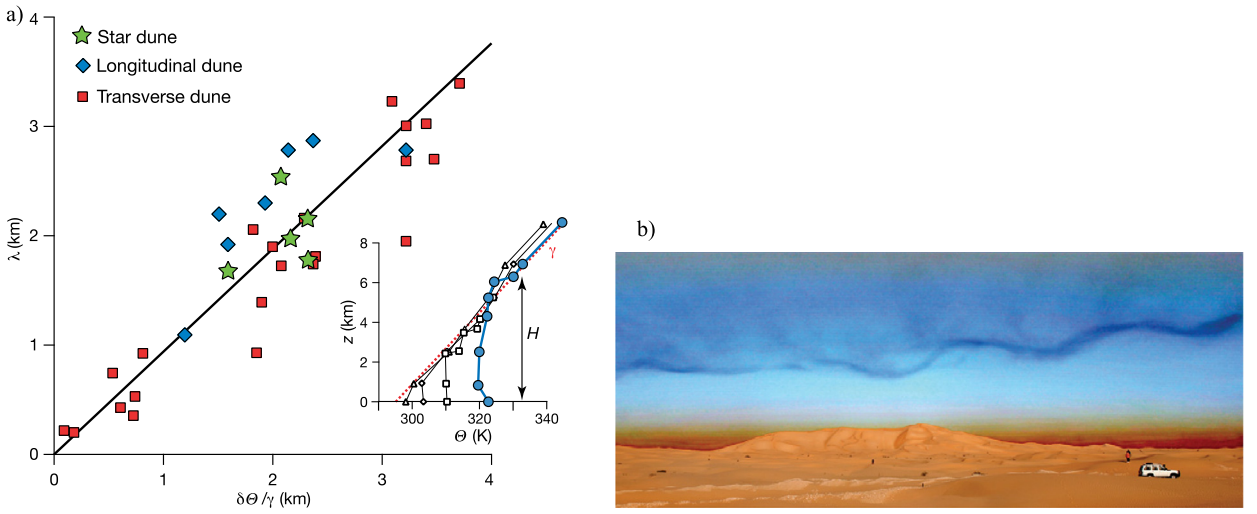

Fig. 7. (Color online.) a) Maximum wavelength λ of dunes as a function of the average mixing height $\delta\Theta/\gamma$. Inset: Virtual potential temperature profiles measured by sounding balloons at noon in Sulayel (South Arabia) at different seasons [52]. The density of air can write as a virtual potential temperature Θ, whose vertical gradient $\mathrm{d}\Theta/\mathrm{d}z = \gamma$ is constant in the stratified free atmosphere. b) Waves propagate on the capping inversion layer above a star dune [52]. The picture was taken a morning of February 2006 in Algeria, which is consistent with a thin atmospheric boundary layer.

4.5. Giant dunes

Andreotti et al. found a correlation between the maximum size of dunes and the local average depth of the atmospheric boundary layer as shown in Fig. 7 [52]. These giant dunes are often referred to as "draas" and concern all dune types mentioned above [59]. In the atmospheric boundary layer, convection takes place because the sun heats the ground. Above, in the free atmosphere, this turbulent mixing is stabilized by the negative vertical density gradient of the air, which induces a restoring buoyancy force. Thus, the height of the mixing layer is set by the heat flux coming from ground and varies in line with seasons and day time. The atmospheric boundary layer is thinner during winter and in the morning, thicker during summer and in the afternoon. In Earth deserts, the average height over the year of this mixing layer depends mainly on the distance to the sea [52].

The correlation between giant dunes length and the average depth of the atmospheric boundary layer can be understood by considering the inviscid potential flow over an undulated bottom ($z = H\cos(kx)$), with a small aspect ratio ($kH \ll 1$). As seen before (Eq. (7)), the flow is in phase with the topography. The perturbation of the flow velocity is positive over bumps and negative over troughs and its magnitude scales with the aspect ratio of the topography. It is maximum at the level of the ground and decreases exponentially with the distance from the bottom on a characteristic length, which is proportional to the wavelength of the topography ($u = U\,[1 + kH\cos(kx)]\exp(-kz)$). It is a general result that a perturbation modifies a field over a characteristic distance, which scales with the perturbation size. For small aspect ratios, the characteristic distance is set by the wavelength only. Without upper bound, it is the inertia of the flow that prevents the perturbation from extending higher than the topography wavelength. The flow perturbation is "confined" to a wavelength height. With an upper bound, if the flow depth is smaller than this characteristic distance, the flow perturbation is confined to the flow depth. The flow velocity at the top of the dunes will increase when the flow depth decreases, which increases the sand transport at the top and prevents the dune from growing further. If the velocity speed-up and the A value increases in Eq. (7), the position of the maximum flow velocity and the shear stress in the turbulent inner layer moves towards the top of the undulated topography. When this position is closer than the characteristic length l_{sat}, the top is a place of erosion instead of deposition. Therefore, it seems reasonable that the maximum length of dunes scales with the flow depth, i.e. the height of the atmospheric boundary layer. This is reminiscent of the cut-off frequency in a waveguide.

Andreotti et al. did the weakly non-linear calculation of the two-dimensional turbulent flow in the mixing layer (i.e. the atmospheric boundary layer) confined between a stratified fluid (the free atmosphere) and a sinusoidal bottom to quantitatively predict the maximum length of giant dunes [52]. At the interface between the atmospheric boundary layer and the free atmosphere (i.e. the capping inversion layer), gravity waves can propagate. Interestingly, they found that for the maximum giant dune height and length, the flow becomes supercritical when passing the dune, i.e. the flow velocity is equal to the velocity of the gravity waves [52]. The streamlines of the flow are then squeezed downstream the topography, which corresponds to a maximum fluid velocity and to a minimum flow depth (the interface deforms) in delay with the topography [52], just like for a shallow water flow over an obstacle [3]. This delay of the maximum fluid velocity is stabilizing (Fig. 1).

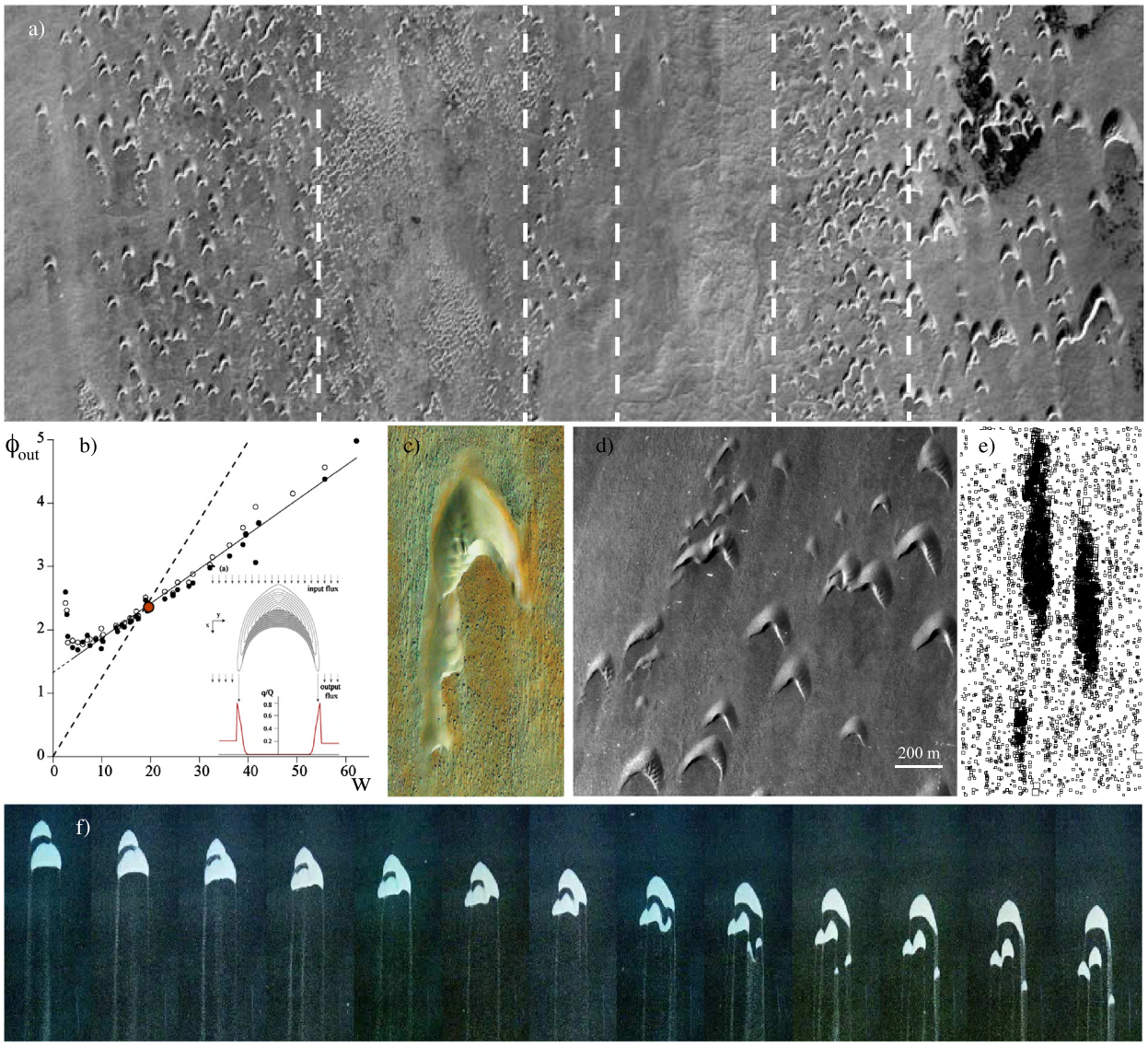

Fig. 8. (Color online.) a) Barchan field in Western Sahara close to Laâyoune (source Pierre Rognon). The wind blows from top (North). The field is structured into corridors. Sparse corridors show large barchans, while dense ones exhibit smaller barchans. b) Instability of an isolated barchan [51,24]. Total sand flux ϕ_{out} that escapes the barchan as a function of barchan width w for a zero incoming flux (black dots) or at constant volume (white dots). The feeding flux ϕ_{in} (dashed line) is strictly proportional to the barchan width. The equilibrium point $\phi_{in} = \phi_{out}$ is unstable. These are numerical results using a model similar to (HerrDiff). Lengths and times are rescaled by l_{sat} and l_{sat}^2/q_{sat} respectively. c) A large barchan calves smaller ones from its horn (from Google Earth, after [85]) d) Detail of the dune field in (a) showing calving and collisions. e) Structured barchan field in an agent-based model [86]. Barchans are squares and their size is magnified. f) Time lapse of a collision between barchans under water. Images are 8 cm wide. In all panels, the flow is coming from the top.

5. Selection of barchans size—dynamics of barchan fields

Whereas giant dunes represent a large part of transverse, linear and star dunes, there are only a few giant barchans [52]. Their size seems to be selected by other mechanisms such as their interactions within a field. In deserts, barchans are not isolated objects but are parts of large dune assemblies as shown in Fig. 8. The very existence of barchan fields seems to conflict with the fact that barchans are unstable on their own (Fig. 8) [51,24]. With an incoming sand flux, a barchan shall capture a volume of sand per unit of time strictly proportional to its width. The height of the transport layer and the saltation length are much smaller than the height and length of the dunes. In contrast, the output sand flux that barchans lose from their horns barely depends on their size and can be considered as a non-zero constant. Depending on the incoming flux, a barchan will either grow or shrink if its size departs from the equilibrium size, which is set by the balance between sand loss and sand capture [51] (Fig. 8b). However, a dune field is not restricted to a sparse desert of giant barchan dunes. Within a field, the size of barchans is widely distributed. Locally, barchans often align in echelon, i.e. the horn

of an upwind dune points towards the back tip of a downwind one. Above all, a barchan field may be non-homogeneous and spatially-structured in narrow corridors, which extend in the wind direction. Dense regions of small barchans and sparse regions of larger barchans coexist, whereas neither the local conditions nor the boundary conditions differ notably [87]. The size of barchans is selected within corridors [87].

Two mechanisms can regulate the barchan size. The first one comes from the bed instability, which develops on the arms of large barchans, when arms are long compared to the initiation length λ_0. As a result, large barchans calve smaller dunes (Fig. 8c). The second one comes from interactions between dunes. Because smaller dunes propagate faster than larger ones (Eq. (16)), dunes collide within a field. Underwater experiments and numerical simulations (HerrDiff) showed that collisions between two dunes lead to the merging or the splitting of dunes into two or several new dunes, depending on their size ratio and on their lateral overlap at collision [88–91] (Fig. 8). Because both mechanisms split dunes into smaller ones, they can account for the stabilization of dune size, as proposed using a mean field approach [89]. In order to investigate the statistical properties and spatial arrangements of dune fields, a numerical model where the barchan is the elementary cell have been developed [90,92,85]. These models implement calving, merging and splitting collisions to identify the mechanisms responsible for size selection and spatial organization.

As expected, the size selection successfully emerges from all numerical models. The local arrangement in echelon is reproduced when barchans lose sand or calve small dunes from their horns [93,85]. However, the self-organization of a dune field into corridors is recovered only when collisions statistically lead to an increasing number of dunes and appears to be a dynamical effect (Fig. 8e) [92,94]. Collisions produce small dunes that are sustained in dense regions by the sand loss of upwind dunes. These small dunes go faster and collide downwind dunes, again producing small dunes in an avalanche-like process. These dense regions are localized in the simulated field. Under stationary but spatially random forcing through dune nucleation, the numerical field reaches a statistical steady state characterized by a constant number of dunes and a stationary size distribution. Nevertheless, dense regions are intermittent and avalanches of collisions look alike bursts whereby the field relaxes a perturbation in dune density [92,94].

6. Conclusion

The physics of dunes raises many interesting questions from the scale of a sand grain to the one of a dune field. The shape and dynamics of dunes do not depend much on the details of sand transport though. Simple mechanisms such as the wind speed-up over the dune topography, its phase shift because of dune slope, the possibility for a linear dune to grow in height or extend in a multidirectional wind regime, yield a consistent picture of the morphodynamics of isolated sand dunes. In many cases, things can be predicted quantitatively so that dunes shape, size and orientation are used to constraint the wind circulation models or sediment grain properties on Mars, Titan or past Earth [76,79,82,95–107]. When dune interactions come into play, the picture is less sharp. The dynamics of closely spaced dunes appear to be partly controlled by the recirculation bubble, for which an accurate description is still missing. However, statistical properties or dynamics of sand dunes assemblies can be successfully recovered while ignoring the details of aerodynamics [108,109,93, 90,92,85]. The dune field or desert scale was left out of the scope of this review and is barely explored on a physical point of view. These natural systems are generally out-of-equilibrium and non-conservative and their understanding would gain from insights of statistical physicists. The dynamics of sandy deserts are a great source of new interesting subjects, e.g. the morphogenesis and evolution of deserts [103,110] or their adaptation to a climatic change affecting wind regimes or boundary conditions.

Acknowledgements

I warmly thank Philippe Claudin, Clément Narteau, Pascal Hersen and Stéphane Douady for their insights and for stimulating discussions. I thank the two editors Alexandre Valance and Michel Louge for their support. The author is financially supported by the French National Research Agency (grant ANR-12-BS05-001/EXODUNES).

References

[1] R.A. Bagnold, The Physics of Blown Sand and Desert Dunes, Chapman and Hall, London, 1941.
[2] R.A. Bagnold, Libyan Sands: Travel in a Dead World, Hodder and Stoughton, London, 1935, Eland, 2010.
[3] E. Guyon, J.P. Hulin, L. Petit, Hydrodynamique Physique, EDP Sciences, 2001.
[4] W. Gong, A. Ibbestson, A wind tunnel study of turbulent flow over model hills, Bound.-Layer Meteorol. 49 (1989) 113–148.
[5] J.D. Iversen, R. Greeley, J. Marshall, J. Pollack, Aeolian saltation threshold: the effect of density ratio, Sedimentology 34 (1987) 699–706, http://dx.doi.org/10.1111/j.1365-3091.1987.tb00795.x.
[6] O. Durán, P. Claudin, B. Andreotti, On aeolian transport: grain-scale interactions, dynamical mechanisms and scaling laws, Aeolian Res. 3 (2011) 243–270, http://dx.doi.org/10.1016/j.aeolia.2011.07.006.
[7] J. Kok, E. Parteli, T. Michaels, D. Bou Karam, The physics of wind-blown sand and dust, Rep. Prog. Phys. 75 (2012) 106901, http://dx.doi.org/10.1063/1.4757662.
[8] J. Ungar, P. Haff, Steady state saltation in air, Sedimentology 34 (1987) 289–299, http://dx.doi.org/10.1111/j.1365-3091.1987.tb00778.x.
[9] P. Gondret, L. Lance, M. Petit, Bouncing motion of spherical particles in fluids, Phys. Fluids 14 (2002) 643–656.
[10] M. Creyssels, P. Dupont, A. Ould el Moctar, A. Valance, I. Cantat, J. Jenkins, J. Pasini, K. Rasmussen, Saltating particles in a turbulent boundary layer: experiment and theory, J. Fluid Mech. 625 (2009) 47–74, http://dx.doi.org/10.1017/S0022112008005491.

[11] Z. Dong, P. Lv, Z. Zhang, G. Qian, W. Luo, Aeolian transport in the field: a comparison of the effects of different surface treatments, J. Geophys. Res. 117 (2012) D09210, http://dx.doi.org/10.1029/2012JD017538.
[12] K. Rasmussen, M. Sorensen, Vertical variation of particle speed and flux density in aeolian saltation: measurement and modeling, J. Geophys. Res. 113 (2008) F02S12, http://dx.doi.org/10.1029/2007JF000774.
[13] P. Owen, Saltation of uniform grains in air, J. Fluid Mech. 20 (1964) 225–242, http://dx.doi.org/10.1016/j.aeolia.2011.06.002.
[14] M. Sørensen, On the rate of aeolian sand transport, Geomorphology 59 (2004) 53–62, http://dx.doi.org/10.1016/j.geomorph.2003.09.005.
[15] T. Ho, A. Valance, P. Dupont, A. Ould El Moctar, Scaling laws in aeolian sand transport, Phys. Rev. Lett. 106 (2011) 094501.
[16] O. Durán, P. Claudin, B. Andreotti, Numerical simulation of turbulent sediment transport, from bed load to saltation, Phys. Fluids 24 (2012) 103306, http://dx.doi.org/10.1016/j.aeolia.2011.07.006.
[17] K. Lettau, H. Lettau, Experimental and micro-meteorological field studies of dune migration, in: K. Lettau, H. Lettau (Eds.), Exploring the World's Driest Climate, University of Wisconsin Press, Madison, 1978, pp. 110–147.
[18] G. Sauermann, K. Kray, H. Herrmann, Continuum saltation model for sand dunes, Phys. Rev. E 64 (2001) 031305, http://dx.doi.org/10.1103/PhysRevE.64.031305.
[19] P. Hersen, S. Douady, B. Andreotti, Relevant length scale for barchan dunes, Phys. Rev. Lett. 89 (26) (2002) 264301.
[20] T. Pahtz, J. Kok, E. Parteli, H. Herrmann, Flux saturation length of sediment transport, Phys. Rev. Lett. 111 (2013) 218002, http://dx.doi.org/10.1103/PhysRevLett.111.218002.
[21] B. Andreotti, P. Claudin, O. Pouliquen, Measurements of the aeolian sand transport saturation length, Geomorphology 123 (2010) 343–348, http://dx.doi.org/10.1016/j.geomorph.2010.08.002.
[22] P. Claudin, G. Wiggs, B. Andreotti, Field evidence for the upwind velocity shift at the crest of low dunes, Bound.-Layer Meteorol. 148 (2013) 195–206.
[23] S. Coleman, B. Melville, Bed-form development, J. Hydraul. Eng. 120 (4) (1994) 5108.
[24] P. Hersen, Morphogenesis and dynamics of barchan dunes, PhD thesis, 2004, https://tel.archives-ouvertes.fr/tel-00008602.
[25] V. Langlois, A. Valance, Initiation and evolution of current ripples on a flat sand bed under turbulent water flow, Eur. Phys. J. E 22 (2005) 201–208.
[26] C. Narteau, D. Zhang, O. Rozier, P. Claudin, Setting the length and time scales of a cellular automaton dune model from the analysis of superimposed bed forms, J. Geophys. Res., Earth Surf. 114 (2009) F3, http://dx.doi.org/10.1029/2008JF001127.
[27] L. Ping, C. Narteau, Z. Dong, Z. Zhang, S. Courrech du Pont, Emergence of oblique dunes in a landscape-scale experiment, Nat. Geosci. 7 (2014) 99–103, http://dx.doi.org/10.1038/ngeo2047.
[28] G. Wiggs, I. Livingstone, A. Warren, The role of streamline curvature in sand dune dynamics: evidence from field and wind tunnel measurements, Geomorphology 17 (1996) 29–46.
[29] J. Finnigan, M. Rauchpach, E. Bradley, G. Aldis, A wind tunnel study of turbulent flow over a two-dimensional ridge, Bound.-Layer Meteorol. 50 (1990) 277–317.
[30] P. Taylor, P. Mason, E.F. Bradley, Boundary-layer flow over low hills (a review), Bound.-Layer Meteorol. 39 (1987) 107–132.
[31] A. Fourrière, River morphodynamics: width selection, ripples and dunes, PhD thesis, 2009, https://pastel.archives-ouvertes.fr/pastel-00005562v1.
[32] F. Charru, B. Andreotti, P. Claudin, Sand ripples and dunes, Annu. Rev. Fluid Mech. 45 (2013) 469–493.
[33] P. Jackson, J. Hunt, Turbulent wind flow over a low hill, Q. J. R. Meteorol. Soc. 101 (1975) 929–955, http://dx.doi.org/10.1002/qj.49710143015.
[34] K. Kroy, G. Sauermann, H. Herrmann, Minimal model for aeolian sand dunes, Phys. Rev. E 66 (3) (2002) 031302.
[35] A. Fourrière, P. Claudin, B. Andreotti, Bedforms in a turbulent stream: formation of ripples by primary linear instability and of dunes by non linear pattern coarsening, J. Fluid Mech. 649 (2010) 287–328, http://dx.doi.org/10.1017/S0022112009993466.
[36] S. Arens, H. Van Kaam-Peters, J. Van Boxel, Air flow over foredunes and implications for sand transport, Earth Surf. Process. Landf. 20 (1995) 315–332.
[37] I. Walker, W. Nickling, Simulation and measurement of surface shear stress over isolated and closely spaced transverse dunes in a wind tunnel, Earth Surf. Process. Landf. 28 (2003) 1111–1124, http://dx.doi.org/10.1002/esp.520.
[38] I. Walker, P. Hesp, R. Davidson-Arnott, B. Bauer, S. Namikas, J. Ollerhead, Response of three-dimensional flow to variations in the angle of incident wind and profile form of dunes: Greenwich dunes, Prince Edward Island, Canada, Geomorphology 105 (2009) 127–138.
[39] B. Andreotti, P. Claudin, S. Douady, Selection of dune shapes and velocities. Part 2: a two-dimensional modeling, Eur. Phys. J. B 28 (2002) 341–352, http://dx.doi.org/10.1140/epjb/e2002-00237-3.
[40] H. Elbelrhiti, P. Claudin, B. Andreotti, Field evidence for surface-wave-induced instability of sand dunes, Nature 437 (2005) 720–723, http://dx.doi.org/10.1038/nature04058.
[41] O. Dauchot, F. Lechénault, C. Gasquet, F. Daviaud, Barchan dunes in the lab, C. R. Mecanique 330 (2002) 185–191.
[42] F. Charru, Selection of the ripple length on a granular bed sheared by a liquid flow, Phys. Fluids 18 (2006) 121508.
[43] K. Pye, H. Tsoar, Aeolian Sand and Sand Dunes, Unwin Hyman, London, 1990.
[44] R. Cooke, A. Warren, A. Goudie, Desert Geomorphology, UCL press, 1993.
[45] I. Walker, W. Nickling, Dynamics of secondary airflow and sediment transport over and in the lee of transverse dunes, Prog. Phys. Geogr. 26 (2002) 47–75, http://dx.doi.org/10.1191/0309133302pp325ra.
[46] P. Hesp, K. Hastings, Width, height and slope relationships and aerodynamics maintenance of barchans, Geomorphology 22 (1998) 193–204.
[47] B. Andreotti, P. Claudin, S. Douady, Selection of dune shapes and velocities. Part 1: dynamics of sand, wind and barchans, Eur. Phys. J. B 28 (2002) 321–339, http://dx.doi.org/10.1140/epjb/e2002-00236-4.
[48] D. Zhang, X. Yang, O. Rozier, C. Narteau, Mean sediment residence time in barchan dunes, J. Geophys. Res. Earth Surf. 119 (3) (2014) 451–463, http://dx.doi.org/10.1002/2013JF002833.
[49] O. Durán, E. Parteli, H. Herrmann, A continuous model for sand dunes: review, new developments and application to barchan dunes and barchan dune fields, Earth Surf. Process. Landf. 35 (2010) 1591–1600, http://dx.doi.org/10.1002/esp.2070.
[50] X. Gao, D. Zhang, O. Rozier, C. Narteau, Transport capacity and saturation mechanism in a real-space cellular automaton dune model, Adv. Geosci. 37 (2014) 47–55, http://dx.doi.org/10.5194/adgeo-37-47-2014.
[51] P. Hersen, K.H. Andersen, H. Elbelrhiti, B. Andreotti, P. Claudin, S. Douady, Corridors of barchan dunes: stability and size selection, Phys. Rev. E 69 (2004) 011304, http://dx.doi.org/10.1103/PhysRevE.69.011304.
[52] B. Andreotti, A. Fourrière, F. Ould-Kaddour, B. Murray, P. Claudin, Giant aeolian dune size determined by the average depth of the atmospheric boundary layer, Nature 457 (2009) 1120–1123, http://dx.doi.org/10.1038/nature07787.
[53] E. Parteli, V. Swämmle, H. Herrmann, L. Monteiro, L. Maia, Profile measurement and simulation of transverse dune field in the Lençóis Maranhenses, Geomorphology 81 (2006) 29–42.
[54] O. Rozier, C. Narteau, A real space cellular automaton laboratory, Earth Surf. Process. Landf. 39 (2014) 98–109.
[55] C. Groh, A. Wierschem, N. Aksel, I. Rehberg, C. Kruelle, Barchan dunes in two dimensions: experimental tests for minimal models, Phys. Rev. E 78 (2008) 021304.
[56] D. Zhang, C. Narteau, O. Rozier, Morphodynamics of barchan and transverse dunes using a cellular automaton model, J. Geophys. Res. 115 (F03) (2010) 41.
[57] M. Baddock, I. Livingstone, G. Wiggs, The geomorphological significance of airflow patterns in transverse dune interdunes, Geomorphology 87 (2007) 332–336.

[58] D. Dee, et al., The era-interim reanalysis: configuration and performance of the data assimilation system, Q. J. R. Meteorol. Soc. 137 (2001) 553–597, http://dx.doi.org/10.1002/qj.828.
[59] N. Lancaster, The development of large aeolian bedforms, Sediment. Geol. 55 (1988) 69–89.
[60] S. Courrech du Pont, C. Narteau, X. Gao, Two modes for dune orientation, Geology 42 (2014) 743–746, http://dx.doi.org/10.1130/G35657.1.
[61] S. Coleman, Wave generation and development on a sandy river bed – discussion, in: Issues and Directions in Hydraulics, Proc. of Iowa Hydraulics Colloquium, 1996, pp. 145–155.
[62] K. Koaukou, P.-Y. Lagrée, Stability of an erodible bed in various shear flows, Eur. Phys. J. B 47 (2005) 115–125.
[63] X. Gao, Development, stability and orientation of dune fields, PhD thesis, 2014.
[64] A. Valance, Nonlinear sand bedform dynamics in a viscous flow, Phys. Rev. E 83 (2011) 036304.
[65] D. Parsons, I. Walker, G. Wiggs, Numerical modelling of flow structures over idealized transverse aeolian dunes of varying geometry, Geomorphology 59 (1) (2004) 149–164.
[66] D. Jerolmack, D. Mohrig, Interactions between bed forms: topography, turbulence and transport, J. Geophys. Res., Earth Surf. 110 (F2) (2005).
[67] E. Reffet, S. Courrech du Pont, P. Hersen, S. Douady, Formation and stability of transverse and longitudinal sand dunes, Geology 39 (6) (2010) 491–494, http://dx.doi.org/10.1130/G30894.1.
[68] E. Parteli, J. Andrade, H. Herrmann, Transverse instability of dunes, Phys. Rev. Lett. 107 (2011) 188001, http://dx.doi.org/10.1103/PhysRevLett.107.188001.
[69] L. Guignier, H. Niiya, H. Nishimori, D. Lague, A. Valance, Sand dunes as migrating strings, Phys. Rev. E 87 (2013) 052206, http://dx.doi.org/10.1103/PhysRevE.87.052206.
[70] D.M. Rubin, R.E. Hunter, Bedform alignment in directionally varying flows, Science 237 (1987) 276–278, http://dx.doi.org/10.1126/science.237.4812.276.
[71] D.M. Rubin, H. Ikeda, Flume experiments on the alignment of transverse, oblique, and longitudinal dunes in directionally varying flows, Sedimentology 37 (1990) 673–684.
[72] E. Parteli, O. Durán, H. Tsoar, V. Schwämmle, H. Herrmann, Dune formation under bimodal winds, Proc. Natl. Acad. Sci. USA 1106 (52) (2009) 22085–22089, http://dx.doi.org/10.1073/pnas.0808646106.
[73] D. Rubin, A unifying model for planform straightness of ripples and dunes in air and water, Earth-Sci. Rev. 113 (2012) 176–185, http://dx.doi.org/10.1016/j.earscirev.2012.03.010.
[74] H. Tsoar, Dynamic processes acting on a longitudinal (seif) sand dune, Sedimentology 30 (4) (1983) 567–578, http://dx.doi.org/10.1111/j.1365-3091.1983.tb00694.x.
[75] I. Livingstone, New models for the formation of linear sand dunes, Geography 73 (1988) 105–115.
[76] M. Telfer, P. Hesse, Palaeoenvironmental reconstructions from linear dune fields: recent progress, current challenges and future directions, Quat. Sci. Rev. 78 (2013) 1–21.
[77] N. Lancaster, Linear dunes, Prog. Phys. Geogr. 6 (1982) 475–504.
[78] H. Tsoar, The formation of seif dunes from barchans – a discussion, Z. Geomorphol. 28 (1984) 99–103.
[79] M. Bourke, N. Lancaster, L. Fenton, E. Parteli, J. Zimbelman, J. Radebaugh, Extraterrestrial dunes: an introduction to the special issue on planetary dune systems, Geomorphology 121 (2010) 1–14, http://dx.doi.org/10.1016/j.geomorph.2010.04.007.
[80] K. Taniguchi, N. Endo, H. Sekiguchi, The effect of periodic changes in wind direction on the deformation and morphology of isolated sand dunes based on flume experiments and field data from the Western Sahara, Geomorphology 179 (2012) 286–299, http://dx.doi.org/10.1016/j.geomorph.2012.08.019.
[81] E. Parteli, O. Durán, M. Bourke, H. Tsoar, T. Pöschel, H. Herrmann, Origins of barchan dune asymmetry: insights from numerical simulations, Aeolian Res. 12 (2014) 121–133.
[82] C. Breed, M. Grolier, J. McCauley, Morphology and distribution of common 'sand' dunes on Mars: comparison with the Earth, J. Geophys. Res., Solid Earth 84 (B14) (1979) 8183–8204, http://dx.doi.org/10.1029/JB084iB14p08183.
[83] N. Lancaster, Star dunes, Prog. Phys. Geogr. 13 (1989) 67–91.
[84] D. Zhang, C. Narteau, O. Rozier, S. Courrech du Pont, Morphology and dynamics of star dunes from numerical modelling, Nat. Geosci. 5 (2012) 463–467, http://dx.doi.org/10.1038/NGEO1503.
[85] S. Worman, A. Brad Murray, R. Littlewood, B. Andreotti, P. Claudin, Modeling emergent large-scale structures of barchan dune fields, Geology 41 (2013) 1059–1062, http://dx.doi.org/10.1130/G34482.1.
[86] M. Génois, Dynamiques d'un système non conservatif: Cas d'un modèle de champ de barkhanes, PhD thesis, 2013, https://tel.archives-ouvertes.fr/.
[87] H. Elbelrhiti, B. Andreotti, P. Claudin, Barchan dune corridors: field characterization and investigation of control parameter, J. Geophys. Res. 113 (2008) F02S15, http://dx.doi.org/10.1029/2007JF000767.
[88] N. Endo, K. Taniguchi, A. Katsuki, Observation of the whole process of interaction between barchans by flume experiments, Geophys. Res. Lett. 31 (2004) L12503.
[89] P. Hersen, S. Douady, Collision of barchan dunes as a mechanism of size regulation, Geophys. Res. Lett. 32 (2005) L21403.
[90] O. Durán, V. Schwämmle, P.G. Lind, The dune size distribution and scaling relations of barchan dune fields, Granul. Matter 11 (1) (2009) 7–11, http://dx.doi.org/10.1007/s10035-008-0120-4.
[91] P. Vermeesch, Solitary wave behavior in sand dunes observed from space, Geophys. Res. Lett. 38 (L22) (2011), http://dx.doi.org/10.1029/2011GL049610.
[92] M. Génois, S. Courrech du Pont, P. Hersen, G. Grégoire, An agent-based model of dune interactions produces the emergence of patterns in deserts, Geophys. Res. Lett. 40 (2013) 1–6, http://dx.doi.org/10.1002/grl.50757.
[93] A. Lima, H. Sauermann, H. Herrmann, K. Kroy, Modelling a dune field, Phys. A, Stat. Mech. Appl. 310 (2002) 487–500.
[94] M. Génois, P. Hersen, S. Courrech du Pont, G. Grégoire, Spatial structuring and size selection as collective behaviours in an agent-based model for barchan fields, Eur. Phys. J. B 86 (2013) 447.
[95] N. Lancaster, G. Kocurek, A. Singhvi, V. Pandey, M. Deynoux, J.-F. Ghienne, K. Lô, Late Pleistocene and Holocene dune activity and wind regimes in the Western Sahara desert of Mauritania, Geology 30 (11) (2002) 991–994.
[96] R. Lorenz, et al., The sand seas of Titan: Cassini radar observations of longitudinal dunes, Science 312 (5774) (2006) 724–727.
[97] P. Claudin, B. Andreotti, A scaling law for aeolian dunes on Mars, Venus, Earth, and for subaqueous ripples, Earth Planet. Sci. Lett. 252 (2006) 30–44.
[98] E. Parteli, O. Durán, H. Herrmann, Minimal size of a barchan dune, Phys. Rev. E 75 (2007) 011301.
[99] B. Andreotti, P. Claudin, Comment on "Minimal size of a barchan dune", Phys. Rev. E 76 (2007) 063301.
[100] R. Lorenz, P. Claudin, B. Andreotti, J. Radebaugh, T. Tokano, A 3 km atmospheric boundary layer on Titan indicated by dune spacing and Huygens data, Icarus 205 (2) (2010) 719–721, http://dx.doi.org/10.1016/j.icarus.2009.08.002.
[101] D. Rubin, P. Hesp, Multiple origins of linear dunes on Earth and Titan, Nat. Geosci. 2 (2009) 653–659.
[102] J. Radebaugh, R. Lorenz, T. Farr, P. Paillou, C. Savage, C. Spencer, Linear dunes on Titan and Earth: initial remote sensing comparisons, Geomorphology 121 (1–2) (2010) 122–132, http://dx.doi.org/10.1016/j.geomorph.2009.02.022.
[103] R. Ewing, A. Peyret, G. Kocurek, M. Bourke, Dune field pattern formation and recent transporting winds in the Olympia Undae Dune Field, north polar region of Mars, J. Geophys. Res. 115 (2010) 1–25.

[104] T. Tokano, Relevance of fast westerlies at equinox for the eastward elongation of Titan's dunes, Aeolian Res. 2 (2010) 113–127.
[105] L. Fenton, T. Michaels, R. Beyer, Inverse maximum gross bedform-normal transport 1: how to determine a dune-constructing wind regime using only imagery, J. Geophys. Res. 117 (2012) F03035, http://dx.doi.org/10.1029/2012JF002368.
[106] N. Bridges, P. Geissler, S. Sivestro, M. Banks, Bedform migration on Mars: current results and future plans, Aeolian Res. 9 (2013) 133–151, http://dx.doi.org/10.1016/j.aeolia.2013.02.004.
[107] A. Lucas, et al., Growth mechanisms and dune orientation on Titan, Geophys. Res. Lett. 41 (17) (2014) 6093–6100, http://dx.doi.org/10.1002/2014GL060971.
[108] B. Werner, Eolian dunes: computer simulations and attractor interpretation, Geology 23 (1995) 1107–1110.
[109] G. Kocurek, R. Ewing, Aeolian dune-field self-organization – implications for the formation of simple versus complex dune-field patterns, Geomorphology 72 (2005) 94–105.
[110] E. Eastwood, J. Nield, A. Baas, G. Kocurek, Modelling controls on aeolian dune-field pattern evolution, Sedimentology 58 (2011) 1391–1406, http://dx.doi.org/10.1111/j.1365-3091.2010.01216.x.